Materials Today Bio 31 (2025) 101605

Contents lists available at ScienceDirect

Materials Today Bio

journal homepage: www.journals.elsevier.com/materials-today-bio

A brief strategy for the preparation of silk fibroin-copper sulfide-based electrospun nanofibrous membranes with photothermal antimicrobial properties to accelerate the infected wound healing

Rui Cai [a,c,1], Jiayu Zhao [a,1], Peirong Zhou [a], Xuemin Ma [a], Chuankai Zhang [a], Zhaodan Wu [a], Liyu Hu [a,c], Yajuan Hu [a], Yongcen Chen [a], Chenglong Huang [a,b,*], Gang Tao [a,c,**]

[a] Luzhou Key Laboratory of Oral & Maxillofacial Reconstruction and Regeneration, The Affiliated Stomatological Hospital, Southwest Medical University, Luzhou, 646000, China
[b] Department of Oral and Maxillofacial Surgery, The Affiliated Stomatological Hospital, Southwest Medical University, Luzhou, 646000, China
[c] Institute of Stomatology, Southwest Medical University, Luzhou, 646000, China

ARTICLE INFO

Keywords:
Copper sulfide nanoparticles
Silk fibroin
Nanofibrous membranes
Photothermal therapy
Wound healing

ABSTRACT

Bacterial infections often hinder the wound-healing process. Antibiotics are commonly used to eradicate bacteria, but long-term use can lead to the development of drug-resistant bacteria. Photothermal therapy (PTT) is a promising technology that utilizes a photothermal agent (PTA) to convert near-infrared radiation into heat, which can eliminate bacteria and has the advantages of being highly effective, controllable, and low drug resistance. In this study, we obtained silk fibroin-copper sulfide nanoparticles(SF/CuS NPs)*in situ* with excellent photothermal responsive properties by a green synthesis strategy using silk fibroin proteins as biological templates. Then, the SF/CuS NPs were mixed with PVA solution, and the photothermal nanofiber membrane (PVA-SF/CuS) was prepared using the electrostatic spinning technique. The synthesized SF/CuS NPs endowed the nanofiber membrane with excellent photothermal sterilization properties. In addition, the constructed PVA-SF/CuS nanofibrous membranes had good cytocompatibility and haemocompatibility. Meanwhile, *in vivo* experiments confirmed that PVA-SF/CuS nanofibrous membrane could inhibit the expression of pro-inflammatory factor (IL-6), promote the expression of angiogenic factor (VEGF), and accelerate collagen deposition and neovascularization under near-infrared light irradiation, which could then promote the healing of infected wounds. Thus, the PVA-SF/CuS nanofiber membrane provides a new candidate material for treating bacterially infected wounds.

1. Introduction

As the human body's largest organ, the skin covers the body surface and directly contacts the external environment [1,2]. It is both the barrier that protects body tissues and organs from external threats and the most vulnerable body organ to external aggression. Skin wounds are a common problem in daily life, and the accompanying accumulation of bacteria at the wound site can lead to serious infections and even life-threatening conditions [3,4]. Currently, infected wounds are managed clinically, mainly through debridement and antibiotic treatment [5]. However, the misuse of antibiotics may lead to the emergence of various drug-resistant bacteria, which is not conducive to building a safe, harmonious healthcare environment [6–8]. Wound dressings are an effective strategy to protect wounds from external damage, but most of the existing wound dressings are not sufficiently antimicrobial to establish a favorable external environment for wound healing [9]. Therefore, developing a dressing with high antimicrobial efficacy and promoting wound healing is imperative to minimize or control wound-related infections.

In recent years, photothermal therapy (PTT) has shown an

* Corresponding author. Department of Oral and Maxillofacial Surgery, The Affiliated Stomatological Hospital, Southwest Medical University, Luzhou, 646000, China.
** Corresponding author. Luzhou Key Laboratory of Oral & Maxillofacial Reconstruction and Regeneration, The Affiliated Stomatological Hospital, Southwest Medical University, Luzhou, 646000, China.
E-mail addresses: 309210243@qq.com (C. Huang), taogang@swmu.edu.cn (G. Tao).
[1] These authors contributed equally to this work.

https://doi.org/10.1016/j.mtbio.2025.101605
Received 5 November 2024; Received in revised form 1 February 2025; Accepted 21 February 2025
Available online 21 February 2025

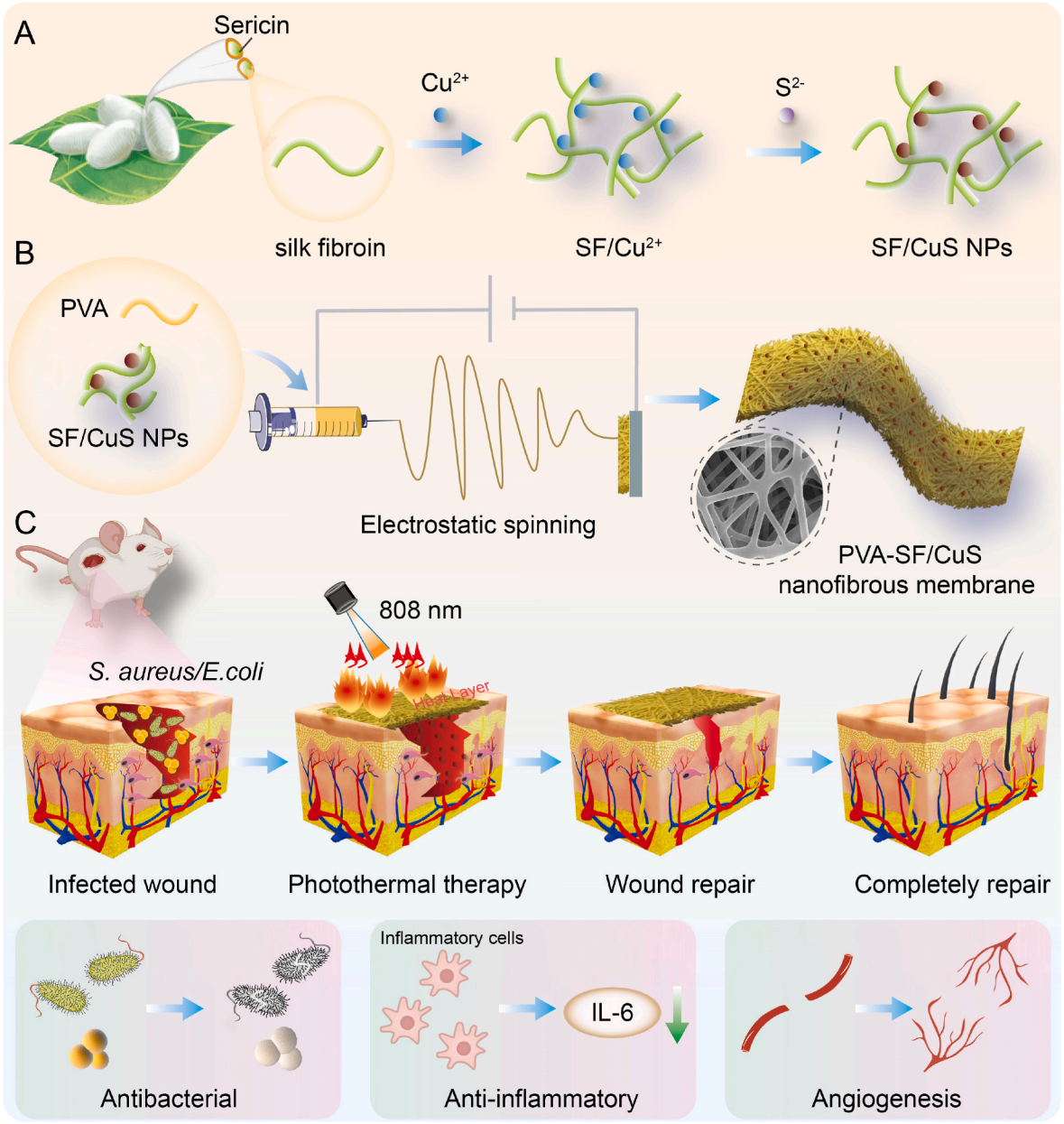

Fig. 1. Schematic diagram of the PVA-SF/CuS composite nanofiber membrane preparation and its application in bacterial infection wound healing. (A) Synthesis of SF/CuS nanoparticles and PVA-SF/CuS composite nanofiber membrane preparation. (B) Application of composite nanofiber membrane in bacterial infection wound healing.

increasingly broad prospect in antimicrobial treatment due to its minimally invasive nature, deep tissue penetration, and immediate therapeutic effect [10,11]. Therefore, adding photothermal agents (PTA) with photothermal effect to existing scaffold materials to kill bacteria around the wound by inducing high temperature through near-infrared (NIR) light irradiation has become a highly effective, drug-resistant, and low systemic toxicity therapeutic method [12,13]. At present, various types of PTAs have been developed, such as indocyanine green [14], polydopamine [15], and inorganic nanoparticles (copper sulfide nanoparticles, gold nanoparticles, carbon-based nanoparticles) [16–18]. Among them, copper sulfide nanoparticles (CuS NPs) are capable of absorbing light in the NIR region (700–1100 nm) and converting it into thermal energy due to the jump between the d-d energy levels of its electrons, which makes it a photothermal agent with good stability, high conversion efficiency and efficient biocompatibility and degradability [19,20]. Moreover, CuS NPs are more easily integrated into biopolymer matrices, such as hydrogels, nanofibrous membranes, and 3D scaffolds. Their small size ensures uniform distribution within the biopolymer matrices, maintaining their structural integrity and functionality. Meanwhile, it has also been shown that copper is an essential trace element, and a specific concentration of Cu^{2+} can promote the proliferation and differentiation of endothelial cells and enhance vasculogenesis, thereby promoting wound healing [21]. However, traditional methods for synthesizing CuS NPs, such as hydrothermal [22], precipitation [23], and emulsion methods [24], are not only demanding in terms of synthesis conditions but also produce polluting substances, consume high amounts of energy and are unfriendly to the environment [25].

In recent years, the *in-situ* synthesis of inorganic nanomaterials using biomolecules as biological templates has attracted widespread attention, as this method has the advantages of low environmental pollution and a convenient preparation process [26–29]. Previous studies have found

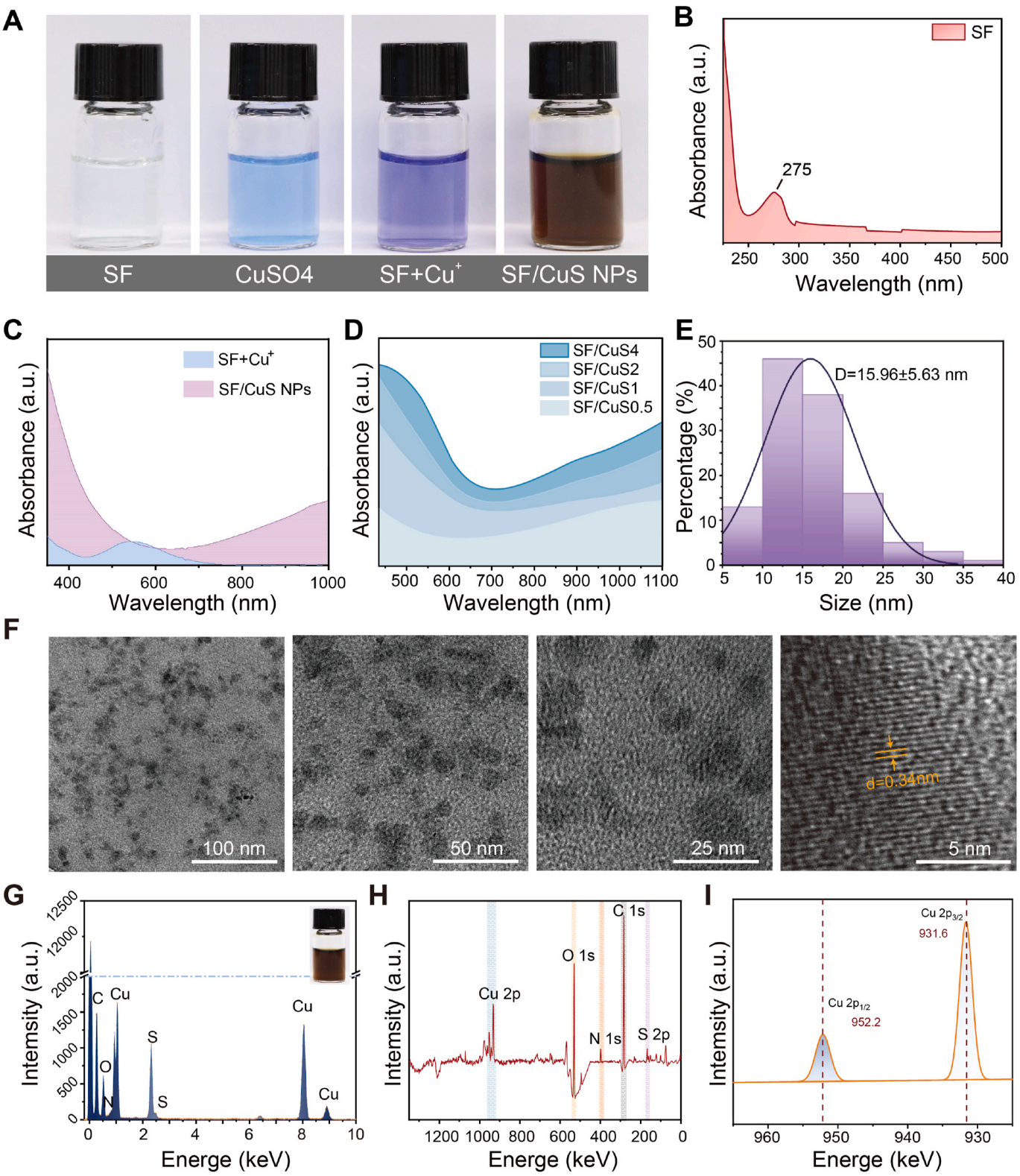

Fig. 2. Synthesis and characterization of SF/CuS NPs. (A) Solution color change during synthesis of SF/CuS NPs. Uv–vis of (B) silk fibroin and (C–D) SF/CuS NPs. (E–F) Particle size and TEM analyses of SF/CuS. (G) EDS and (H–I) XPS analyses of SF/CuS.

that biomass molecules containing many hydroxyl groups can successfully synthesize CuS NPs under general conditions simply [19]. For example, Zhang et al. prepared uniformly dispersed CuS nanoparticles using BSA as a stabilizer [30]. In general, the main structure of silk fibroin protein extracted from cocoons of domestic silkworms is (Gly-Ser-Gly-AlaGly-Ala)n, which contains a sufficient amount of serine (Ser) and tyrosine (Tyr), and it can also be used to synthesize CuS nanoparticles successfully by providing abundant hydroxyl gap-limiting valve effect [20]. In addition, silk fibroin protein is a biocompatible material, especially for skin regeneration, which not only supports cell

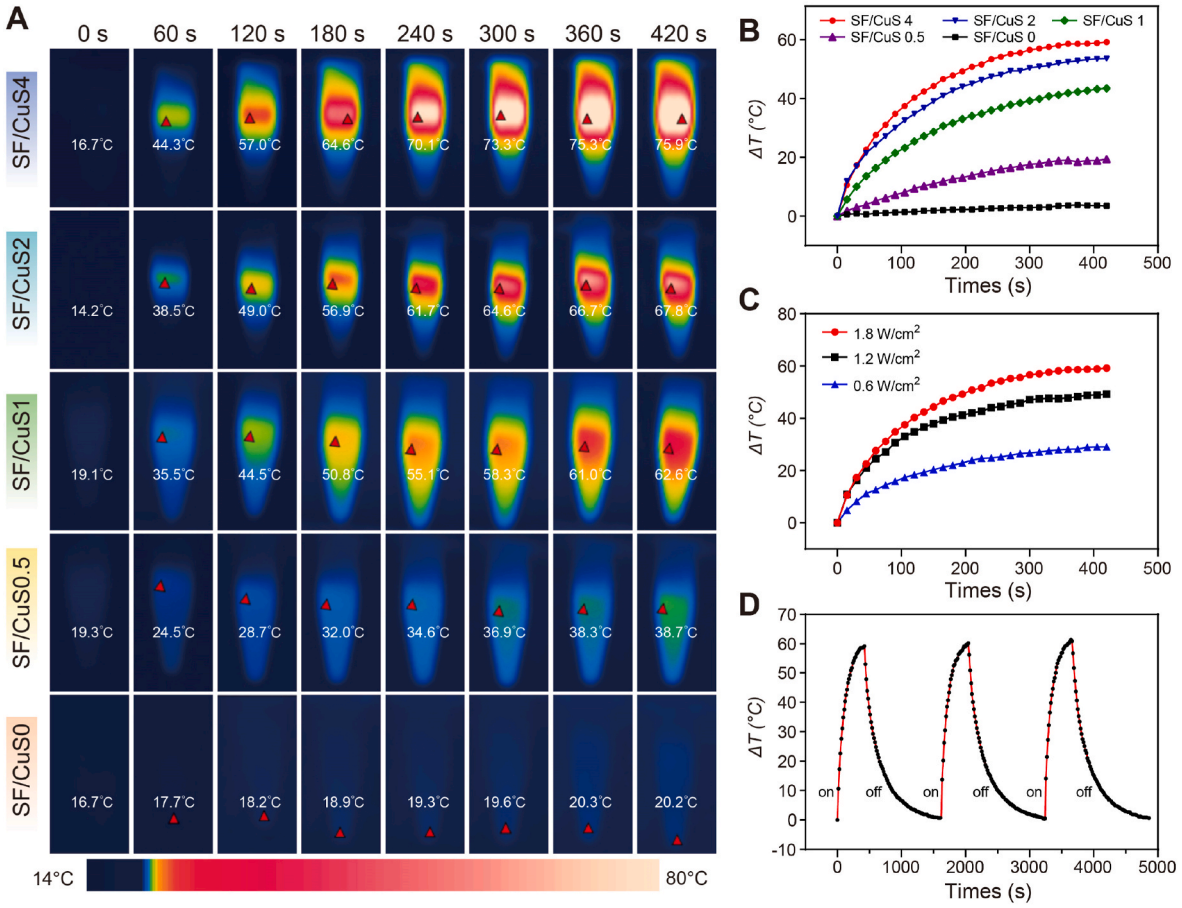

Fig. 3. Photothermal properties of CuS solutions. (A–B) Infrared images and temperature profiles of different concentrations of SF/CuS under 808 nm (1.8 W/cm^2) laser irradiation. (C) Temperature profiles of SF/CuS4 under near-infrared irradiation with different powers (1.8 W/cm^2, 1.2 W/cm^2, and 0.6 W/cm^2). (D) Photothermal stabilization of SF/CuS4 after three consecutive switching cycles under NIR irradiation at 808 nm (1.8 W/cm^2).

recruitment but also promotes the proliferation of skin fibroblasts and facilitates epithelial re-formation, providing a role in facilitating the wound healing process [31,32]. Therefore, we speculate that silk fibroin can serve as a potential biological macromolecule template for the synthesis of CuS NPs and can be used to prepare silk fibroin-copper sulfide nanoparticles *in situ* and in a green and environmentally friendly way.

Generally, various dressings, such as hydrogels, sponges, porous foams, microspheres, and nanofibers, have been developed to promote wound healing [33–35]. Among them, nanofibers prepared by electrostatic spinning have become a wound dressing of interest due to their large surface area/volume ratio, high porosity, small pore size, and structure similar to natural extracellular matrix (ECM) [36–38]. Silk fibroin proteins are suitable for nanofiber dressings due to their good biocompatibility, biodegradability, and easy accessibility [39]. However, the use of silk fibroin alone for the preparation of nanofibers requires the use of highly toxic organic solvents. Polyvinyl alcohol (PVA) has excellent biocompatibility, and a PVA solution with suitable concentration can be used to prepare nanofibers by electrostatic spinning [40,41]. Therefore, we proposed to load CuS in a blend of silk fibroin (SF) and polyvinyl alcohol (PVA) as a non-toxic spinning solution to prepare nanofibers by electrostatic spinning. SF/CuS NPs can be evenly dispersed in electrospun membranes formed by PVA and SF, enabling the PVA-SF/CuS nanofibrous membranes to possess stable photothermal antibacterial properties. At the same time, a specific concentration of Cu^{2+} is uniformly released, which can promote the secretion of VEGF by HUVECs and accelerate the healing of infected wounds [42,43].

In this study, we first prepared silk fibroin-copper sulfide nanoparticles in a facile and environmentally friendly way using silk fibroin protein as a biological template and demonstrated its excellent photothermal properties (Fig. 1A). Then, PVA-SF/CuS nanofibrous membranes with photothermal properties were prepared by mixing the facilely prepared CuS nanoparticles with PVA and silk fibroin solution *via* electrostatic spinning (Fig. 1B). The PVA-SF/CuS nanofibrous membrane has excellent cytocompatibility and haemocompatibility, and due to the photothermal properties of the CuS nanoparticles, the nanofibrous membranes can effectively kill bacteria under near-infrared light. This study confirms that our synthesized SF/CuS NPs have the advantages of being green, safe, stable, and having good antimicrobial performance. The growth of the CuS network can provide excellent photothermal performance. The introduction of SF enhances CuS's hydrophilicity. In addition, it prevents aggregation, which enables SF/CuS NPs to be more uniformly dispersed within the nanofibrous membrane. The PVA-SF/CuS nanofibrous membrane was further demonstrated to effectively inhibit the expression of pro-inflammatory factors and promote the expression of the angiogenic factor, thereby accelerating the healing of infected wounds through a rat skin defect infection model (Fig. 1C). It is also suitable for other carrier substances and has a high potential for application in the future.

2. Materials and methods

2.1. Materials

Silkworm cocoons were purchased from the Sirei Cultural Research Institute (Jiangsu, China). Sodium carbonate, lithium bromide, copper

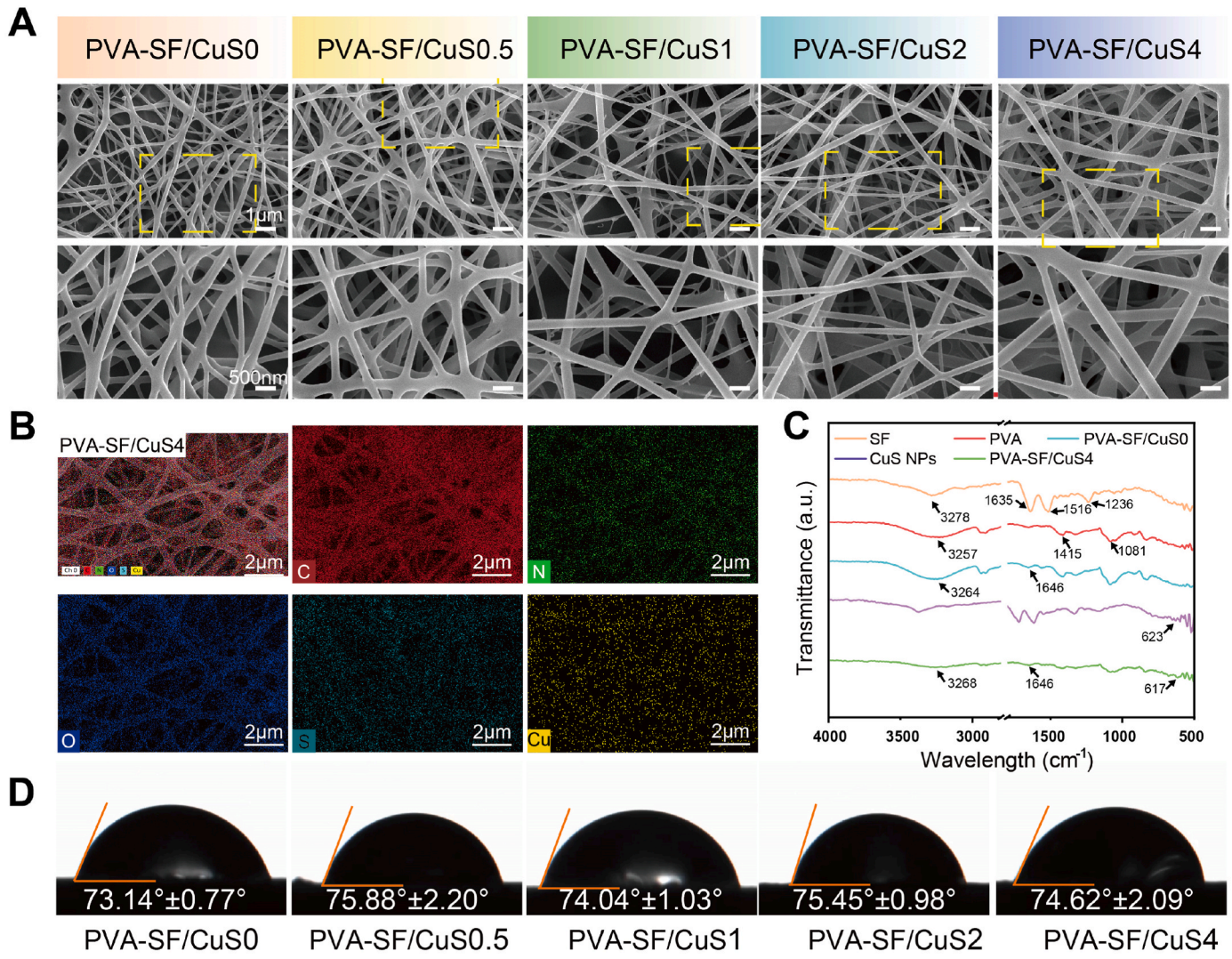

Fig. 4. Characterization of PVA-SF/CuS nanofiber membrane. (A) SEM observation of PVA-SF/CuS nanofiber membrane. (B) Elemental analysis of PVA-SF/CuS4 nanofiber membrane. (C) FTIR spectrum analysis. (D) Contact angle analysis of PVA-SF/CuS nanofiber membrane.

sulfate pentahydrate ($CuSO_4{\cdot}5H_2O$), aqueous ammonium hydroxide ($NH_3{\cdot}H_2O$), sodium sulfate hydrate ($Na_2S{\cdot}9H_2O$), and PVA were purchased from Aladdin Corp (Shanghai, China). All other chemical reagents such as Dulbecco's modified eagle medium (DMEM, Gibco, USA), Roswell Park Memorial Institute 1640 medium (RPMI 1640, Gibco, USA), Fetal bovine serum (FBS, Gibco, USA), 0.25 % Trypsin-EDTA (Gibco, USA), Cell Counting Kit (CCK-8, Beyotime, China), 1 % penicillin-streptomycin (CCK-8, Beyotime, China), Live/Dead® Viability Kit and Live/Dead bacterial staining kits (Thermo Fisher Scientific, USA), were used directly.

2.2. Preparation of silk fibroin (SF)

Silk proteins can be extracted using previous methods [29,44]. To remove the silk sericin, cocoons can be placed in a ratio of 1:100 in 0.5 wt% $NaCO_3$ solution and heated to boiling 30 min later with deionized water rinsed thoroughly. Then, 10 g of the above-degummed silk fibroin was placed in 9.3 mol/L LiBr solution and heated at 60 °C for 30 min. The solution was transferred into a dialysis bag (MW 8000–14000 Da) and dialyzed with deionized water for 3 days. The final product was centrifuged to remove impurities. Finally, the resulting supernatant was freeze-dried to obtain the desired regenerated silk fibroin protein product.

2.3. Synthesis of SF/CuS NPs

A facile synthesis was adopted to prepare CuS NPs with uniform distribution and similar sizes and to reduce reaction energy consumption. Briefly, $NH_3{\cdot}H_2O$ (7 mol/L, 100 μL) was added dropwise to $CuSO_4$ solution (80 mM, 2 mL) until a dark blue solution containing a large amount of $[Cu(NH_3)_4]^{2+}$ was formed. The prepared 4 wt% SF solution (10 mL) was added to it and stirred for 30 min. At this point, the color changed to purple, which signaled the success of the reaction. Then, 4 mol/L of $Na_2S{\cdot}9H_2O$ was added to the mixture and stirred continuously until the solution turned brown. Finally, deionized water was added to 40 mL to obtain a solution of SF/CuS NPs (4 mmol/L), named SF/CuS4. All the reactions were carried out at room temperature. SF/CuS2, SF/CuS1, SF/CuS0.5, and SF/CuS0 were prepared using the same method, changing only the content of the $CuSO_4$ solution.

2.4. Characterization of SF/CuS NPs

The absorption spectra of SF solution, SF + $CuSO_4$ solution, and SF/CuS NP solutions were measured in the 200–1100 nm range using a UV–vis spectrophotometer (TU-1810, Shanghai, China), respectively. The micromorphology and trace composition of SF/CuS NPs were examined using transmission electron microscopy (TEM, JEM-2100,

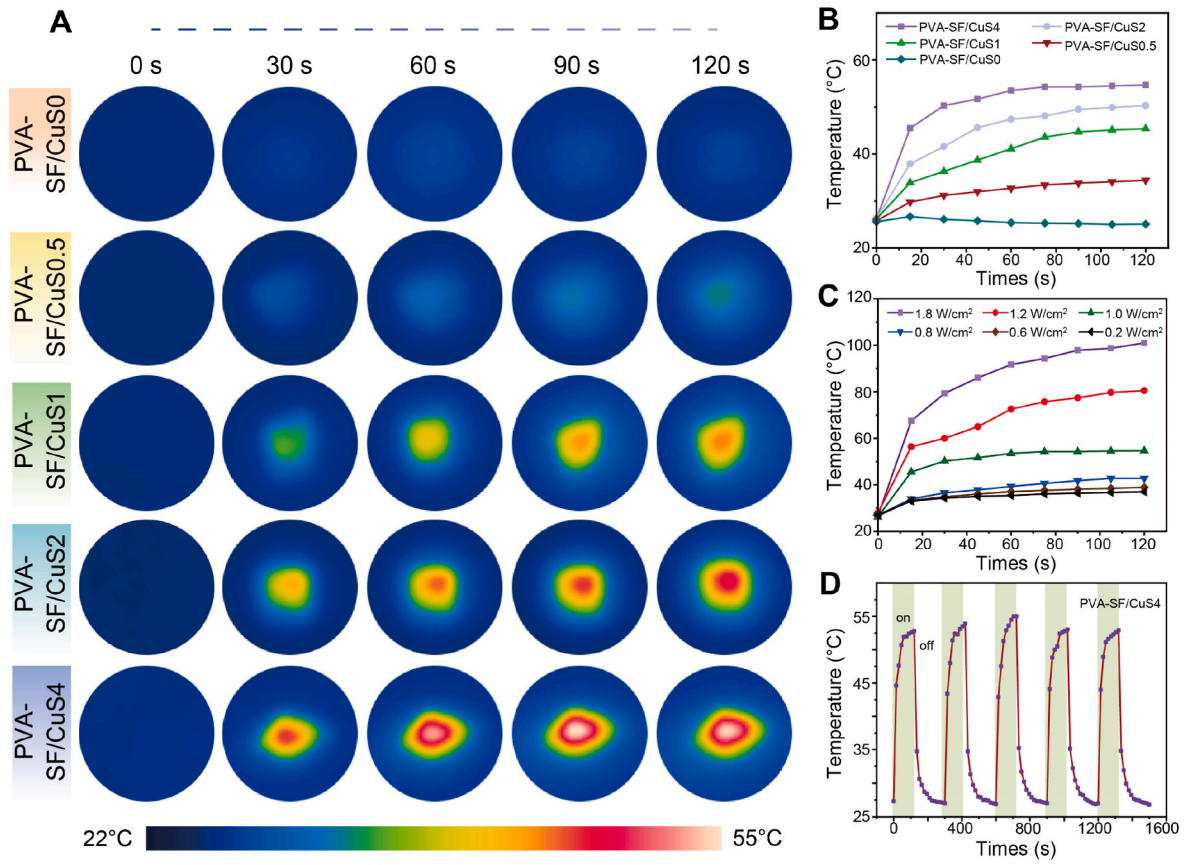

Fig. 5. Near-infrared photothermal performance of PVA-SF/CuS nanofiber membranes *in vitro*. (A) Infrared images and (B) temperature profiles of PVA-SF/CuS nanofiber membranes under 808 nm (1.0 W/cm^2) laser irradiation. (C) Temperature profiles of PVA-SF/CuS4 under near-infrared irradiation with different powers (0.2–1.8 W/cm^2). (D) Photothermal stabilization of PVA-SF/CuS4 after five consecutive switching cycles under NIR irradiation at 808 nm (1.0 W/cm^2).

Tokyo, Japan) and energy dispersive broadspectroscopy (EDS). X-ray photoelectron spectroscopy (XPS, Shimadzu Kratos AXIS Ultra DLD, Nagoya, Japan) was utilized to study the elemental composition and valence distribution of SF/CuS NPs. The crystal structure of SF/CuS NPs was determined using X-ray diffraction (XRD, Ultima4, Japan). The thermogravimetric analysis (TGA) was conducted using a heating rate of 10 °C/min, ranging from room temperature to 800 °C. The weight loss was recorded to assess the sample's thermal stability and decomposition behavior.

2.5. Photothermal property and photothermal stability of SF/CuS NPs

SF/CuS NPs (SF/CuS4 NPs, SF/CuS2 NPs, SF/CuS1 NPs, SF/CuS0.5 NPs, and SF/CuS0) were vertically irradiated with 808 nm laser at a power of 1.8W/cm^2. The irradiation lasted 7 min, and infrared thermal images and temperature changes were recorded using an infrared thermography camera (FLIR, E8-XT, Wilsonville, OR, USA). To determine the optimal laser irradiation power for photothermal conversion, lasers with different powers (1.8W/cm^2, 1.2W/cm^2, 0.6W/cm^2) were used to treat the SF/CuS4 NP solutions following the same procedure. The photothermal efficiency was evaluated based on temperature recordings, and the photothermal stability of SF/CuS4 NPs was assessed over five lasers on/off cycles.

2.6. Fabrication of PVA-SF/CuS composite nanofibrous membranes

Nanofiber membranes were prepared using the electrostatic spinning technique. Briefly, PVA was added to the previously synthesized SF/CuS0 NP solution and completely dissolved. Then, the nanofibrous membranes were prepared by an electrostatic spinning apparatus named PVA-SF/CuS0. The mass fraction of PVA was 7.5 %. The electrospinning process was carried out using a 22 G needle with the distance between the tip of the needle and the collector set at 15 cm. The positive pressure was set to 18.25 kV, and the negative pressure to 2.75 kV. 10 mL of the mixed solution was used, and the feed rate was set at 0.1 mm/min. SF/CuS0.5, SF/CuS1, SF/CuS2, and SF/CuS4 solutions were used instead of SF/CuS0 to obtain PVA-SF/CuS0.5, PVA-SF/CuS1, PVA-SF/CuS2, and PVA-SF/CuS4 nanofiber membranes, respectively.

2.7. Characterization of PVA-SF/CuS composite nanofibrous membranes

PVA-SF/CuS nanofiber membranes were characterized for their morphology and microstructure using field emission scanning electron microscopy (FE-SEM, JSM-7800F, Tokyo, Japan). The elemental composition of the fiber membranes was detected and verified using energy-dispersive X-ray Spectroscopy (EDX) mapping. To assess and identify the molecular bonds and functional groups in the fiber membranes, FTIR spectroscopy was utilized to measure their molecular composition (WQF-530, Beijing, China). Furthermore, the contact angle (CA) of the PVA-SF/CuS nanofiber membranes was measured using a contact angle goniometer (DSA30, Kruss, Germany) to evaluate the hydrophilicity of the nanofiber membranes.

The nanofiber membranes were cut into 1.5 × 1.5 cm squares and immersed in phosphate buffered saline (PBS) solution for 5 days at room temperature to observe the degradation of the nanofiber membranes. After each predetermined period, the nanofiber membranes were removed from the solution, and the water on the surface of the nanofiber membranes was sucked out with filter paper and then weighed. To assess the degree of degradation, the relative weight of the nanofiber membranes is calculated using the following formula:

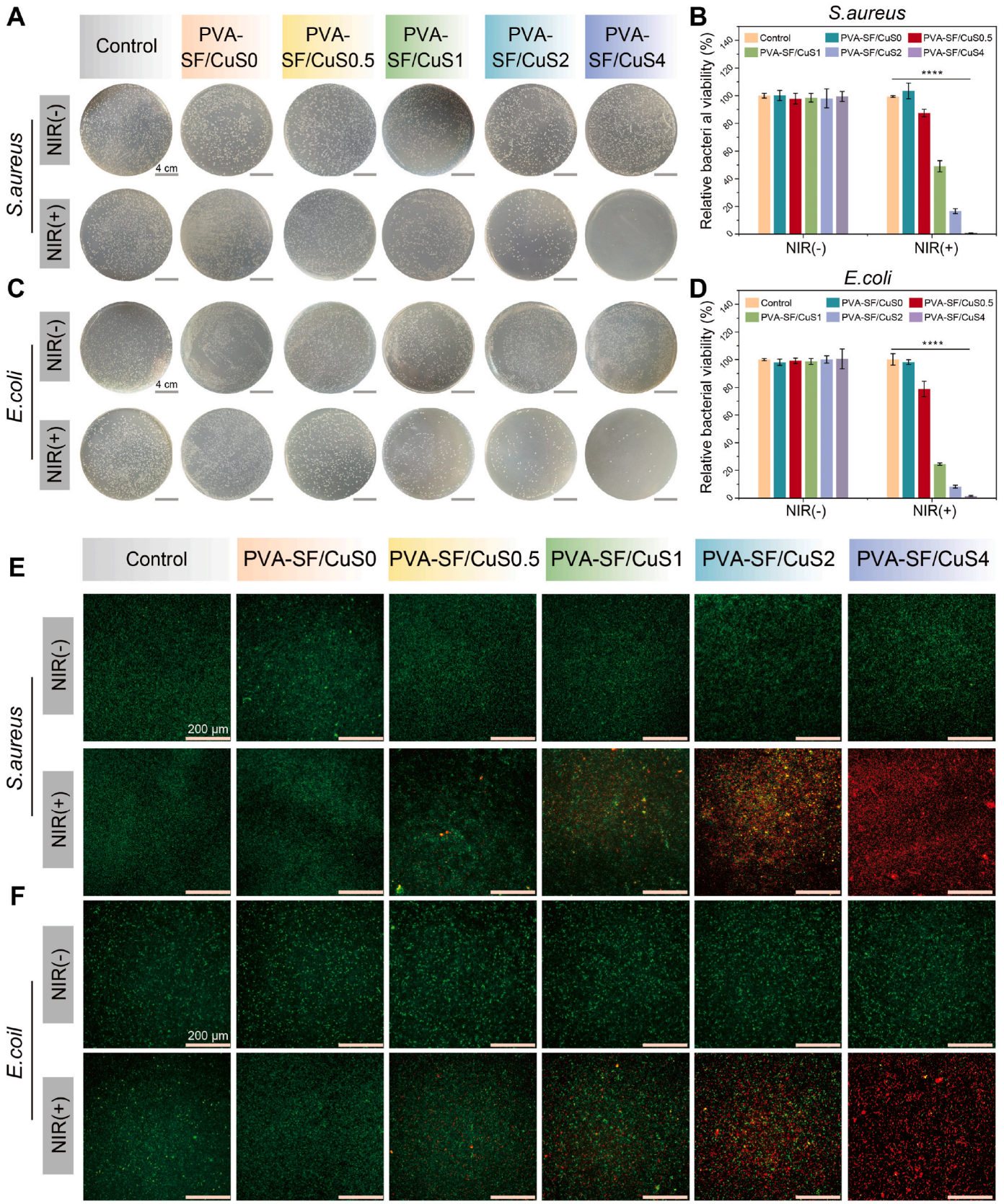

Fig. 6. Antibacterial activity of PVA-SF/CuS nanofiber membranes against *S. aureus* and *E. coli*. (A) Representative images and (B) counting statistics of *S. aureus* colony-forming units with NIR and without NIR irradiation. (C) Representative images and (D) counting statistics of *E. coli* colony-forming units with NIR and without NIR irradiation. Live/dead bacteria staining of *S. aureus* (E) and *E. coli* (F) after being treated with PVA-SF/CuS4 nanofiber membrane with or without NIR irradiation.

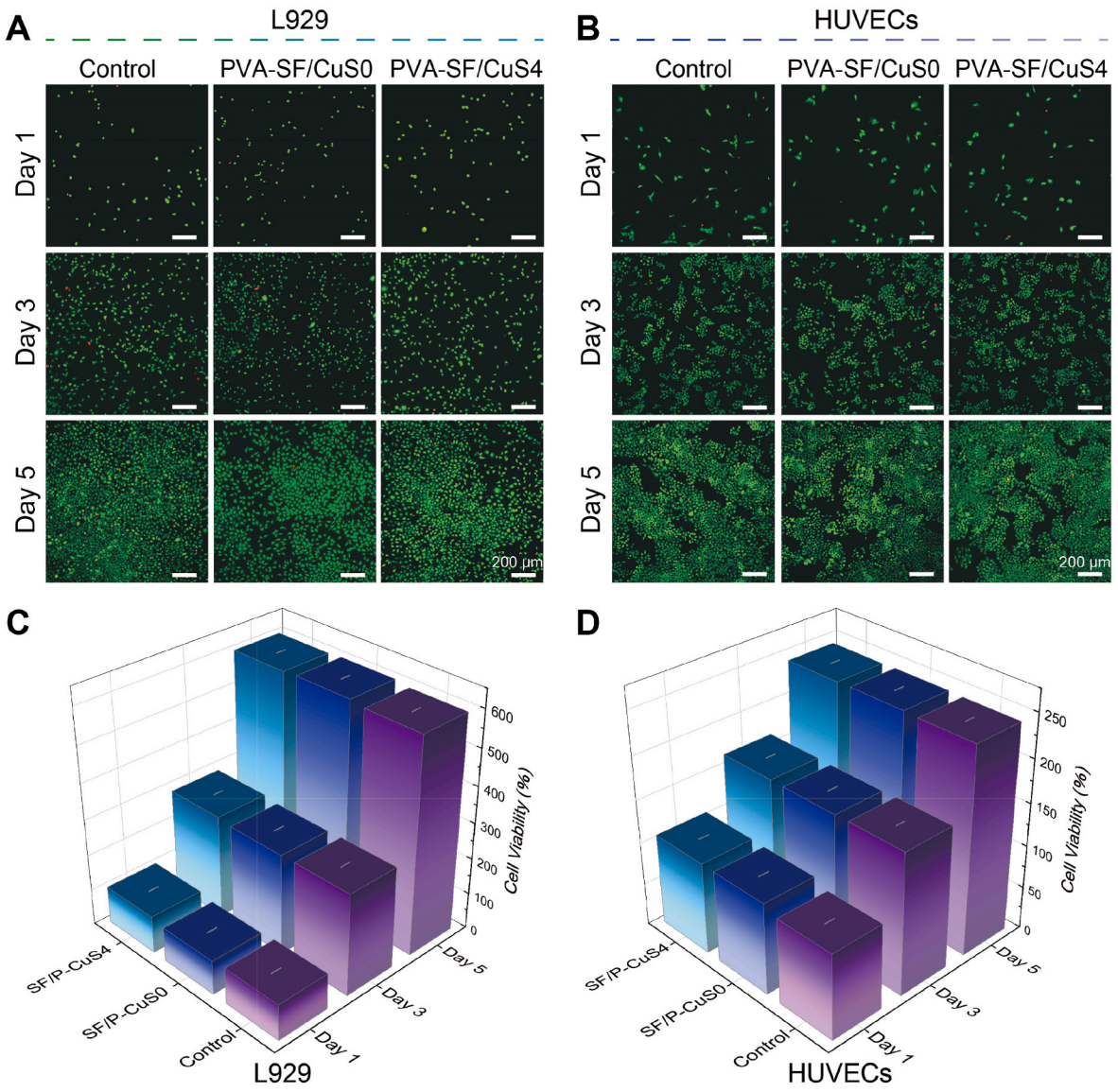

Fig. 7. Cytocompatibility analysis of PVA-SF/CuS nanofiber membranes. (A–B) Live/dead cell staining. (C–D) CCK-8 analysis.

$$\text{Relative weight}(\%) = \frac{Wt}{W0} \times 100\%$$

The weight of the nanofiber membranes (W0) is measured prior to testing. After each impregnation period, the nanofiber membranes are extracted from the impregnating solution and dried until the weight (Wt) remains constant.

2.8. Photothermal property and photothermal stability of PVA-SF/CuS composite nanofibrous membranes

The PVA-SF/CuS composite nanofibers were cut into square pieces of 1 cm × 1 cm and placed in a six-well plate. Subsequently, the nanofiber samples were irradiated with an 808 nm laser at a power density of 1 W/cm^2 for 2 min. During the process, PVA-SF/CuS nanofibrous membranes were irradiated with lasers of different power densities (1.8, 1.6, 1, 0.8, 0.6, 0.2 W/cm^2), and the temperature changes of the composite nanofibrous membranes were recorded using an infrared thermal imager (FLIR, E8-XT, Wilsonville, OR, USA). Finally, the photothermal stability of the PVA-SF/CuS nanofibrous membranes was evaluated under five laser on/off cycles.

2.9. In vitro antibacterial experiment

The nanofiber membrane samples were placed in separate wells of a six-well plate, and 200 μL of *S. aureus* and *E. coli* suspensions (1×10^6 CFU/mL) were added to each sample. Each sample type was divided into groups: Group L(+) for light irradiation or Group L(−) for no light irradiation. For the light irradiation group, the plate was exposed to 808 nm laser light for 2 min at a vertical distance of 15 cm, with a laser power density of 1 W/cm^2. A bacterial suspension containing only PBS was used as the control group, and the same procedures were used for the experimental groups. After diluting the bacterial suspensions 20 times, they were plated on an LB agar medium and incubated at 37 °C for 24 h. The colonies on the plates were then counted and photographed. The relative bacterial viability of each sample was calculated using the following formula:

$$\text{Relative bacterial viability}(\%) = \frac{NS}{N0} \times 100\%$$

Where N0 represents the bacterial count of the control group without light irradiation, and Ns represents the bacterial count of the sample.

Additionally, the bacterial suspensions mentioned above were

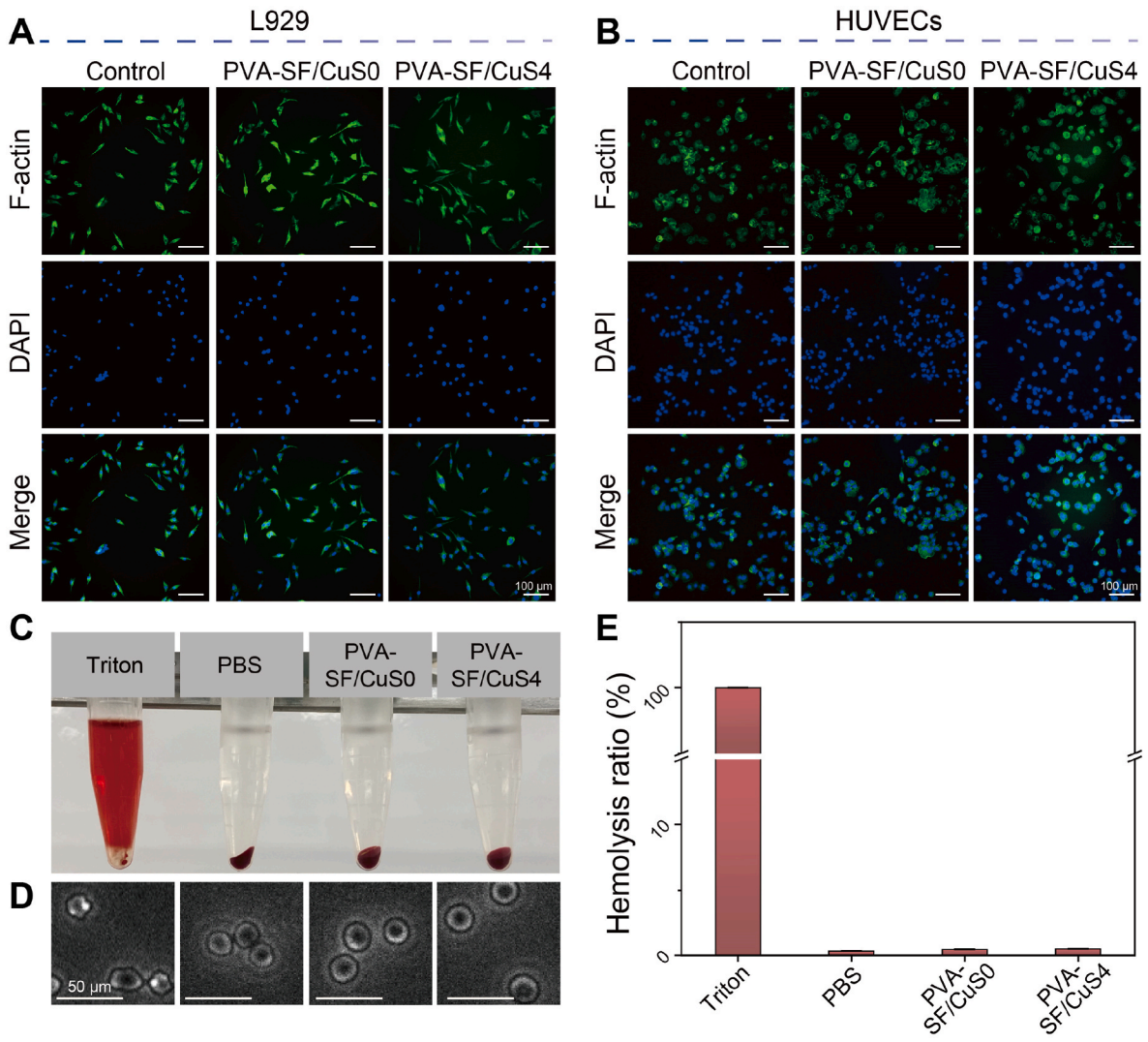

Fig. 8. Biocompatibility analysis of PVA-SF/CuS nanofiber membranes. (A–B) FITC-Phalloidin staining. (C–E) Hemocompatibility testing.

treated with Live/Dead bacterial staining kits. Live bacteria (green color) and dead bacteria (red color) were imaged using a fluorescence microscope.

2.10. *In vitro cell cytocompatibility assay*

Mouse fibroblast cells (L929) were cultured in 1640 medium, and human umbilical vein endothelial cells (HUVECs) were cultured in Dulbecco's modified eagle medium (DMEM), both supplemented with 10 % fetal bovine serum (Gibco). L929 and HUVECs in the logarithmic growth phase were seeded into a 96-well plate, respectively, and cultured at 37 °C with 5 % CO_2 for 24 h. Subsequently, the nanofiber membrane samples were sterilized with ethanol and UV light, and extraction solutions were prepared. Specifically, the nanofiber membrane samples were immersed in fresh 1640 and DMEM in proportion for 24 h, and fresh 1640 and DMEM were used as blank control groups. Then, 100 μL of the fiber membrane extraction solution was used to replace the original culture medium in each well, and the cells were cultured for 5 days. On days 1, 3, and 5, the cells were stained for viability using live/dead staining and observed under a fluorescence microscope. In addition, the cell viability was determined and calculated using the CCK8 method and the following formula:

$$\text{Cell viability } (\%) = \frac{\text{OD(sample} - \text{blank)}}{\text{OD (control} - \text{blank)}} \times 100\%$$

Where OD represents the optical density of the culture plate solution at 545 nm, which is used to assess the fiber membrane samples.

Cells cultured for 3 days were collected and treated with 0.5 % Triton X-100 for 5 min. They were then stained with a FITC-Phalloidin solution for 0.5 h, washed with PBS three times, and stained with DAPI for 30 s. Finally, the cells were visualized using a fluorescence microscope.

2.11. *Hemolysis test*

According to previous methods, hemolysis experiments were performed by collecting sufficient fresh whole blood from healthy SD rats [45]. The PVA-SF/CuS0 nanofiber membrane and PVA-SF/CuS4 nanofiber membrane extraction solutions were mixed with the blood in test tubes. The tubes were then incubated at 37 °C in a water bath for 1 h. Blood treated with Tritonx-100 reagent was used as a positive control, and blood diluted with PBS served as a negative control. Subsequently, the morphology of red blood cells in each group was observed using microscopy. The tubes were then centrifuged for 5 min, and the absorbance (OD) of the supernatant was measured to estimate the hemoglobin content. The hemolysis percentage was calculated using the following equation:

$$\text{Hemolysis } \textit{ratio}(\%) = \frac{\text{ODS} - \text{ODN}}{\text{ODP} - \text{ODN}} \times 100\%$$

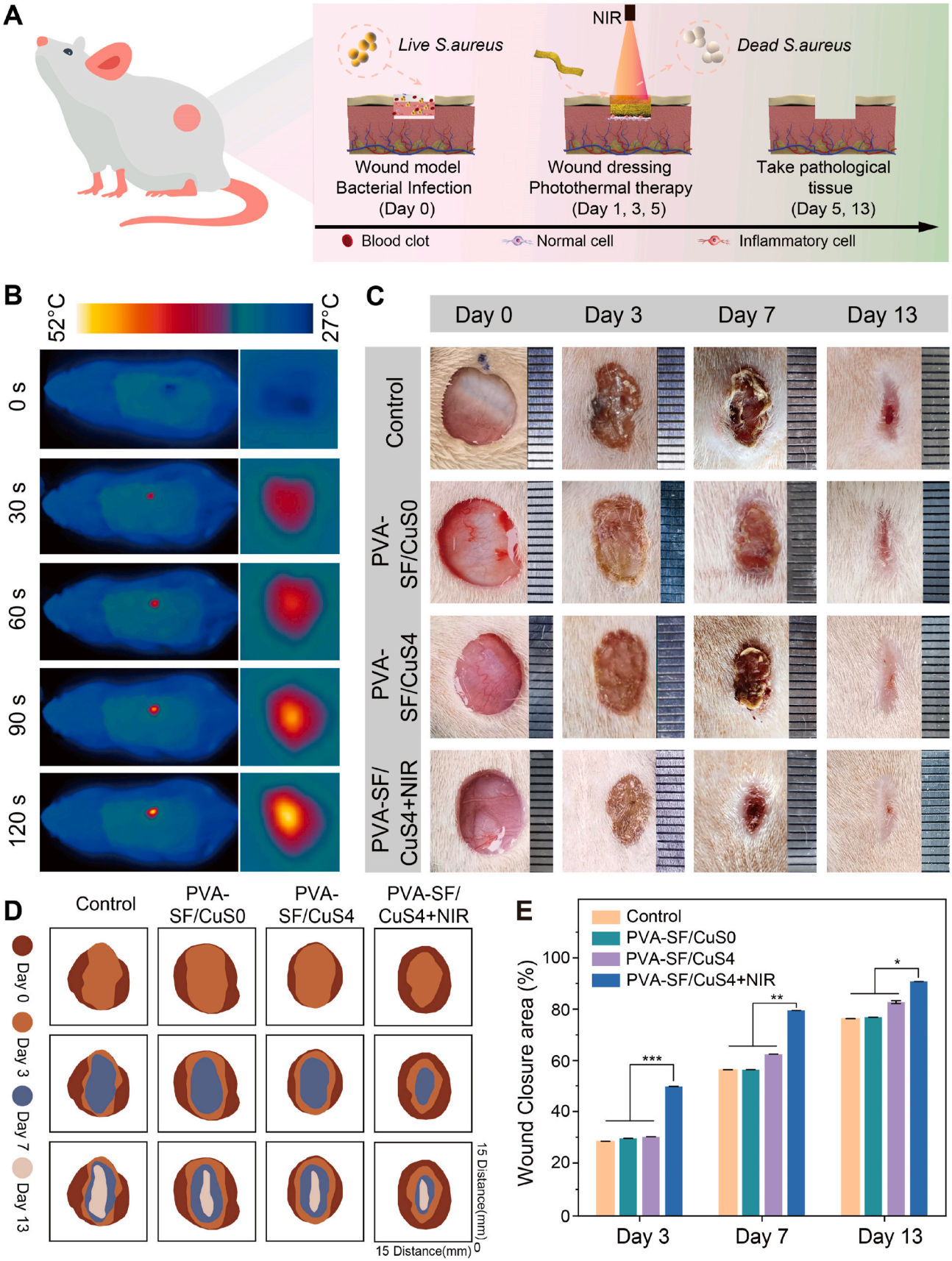

Fig. 9. The efficacy of PVA-SF/CuS nanofiber membrane in treating infected wounds. (A) Schematic diagram of *S. aureus* infected wound model and nanofiber membrane treatment. (B) Photothermal image of PVA-SF/CuS4 nanofiber membrane under NIR irradiation. (C) Pictures and (D) schematics of wound healing on days 0, 3, 7, and 13. (E) Wound healing rates at days 0, 3, 7, and 13.

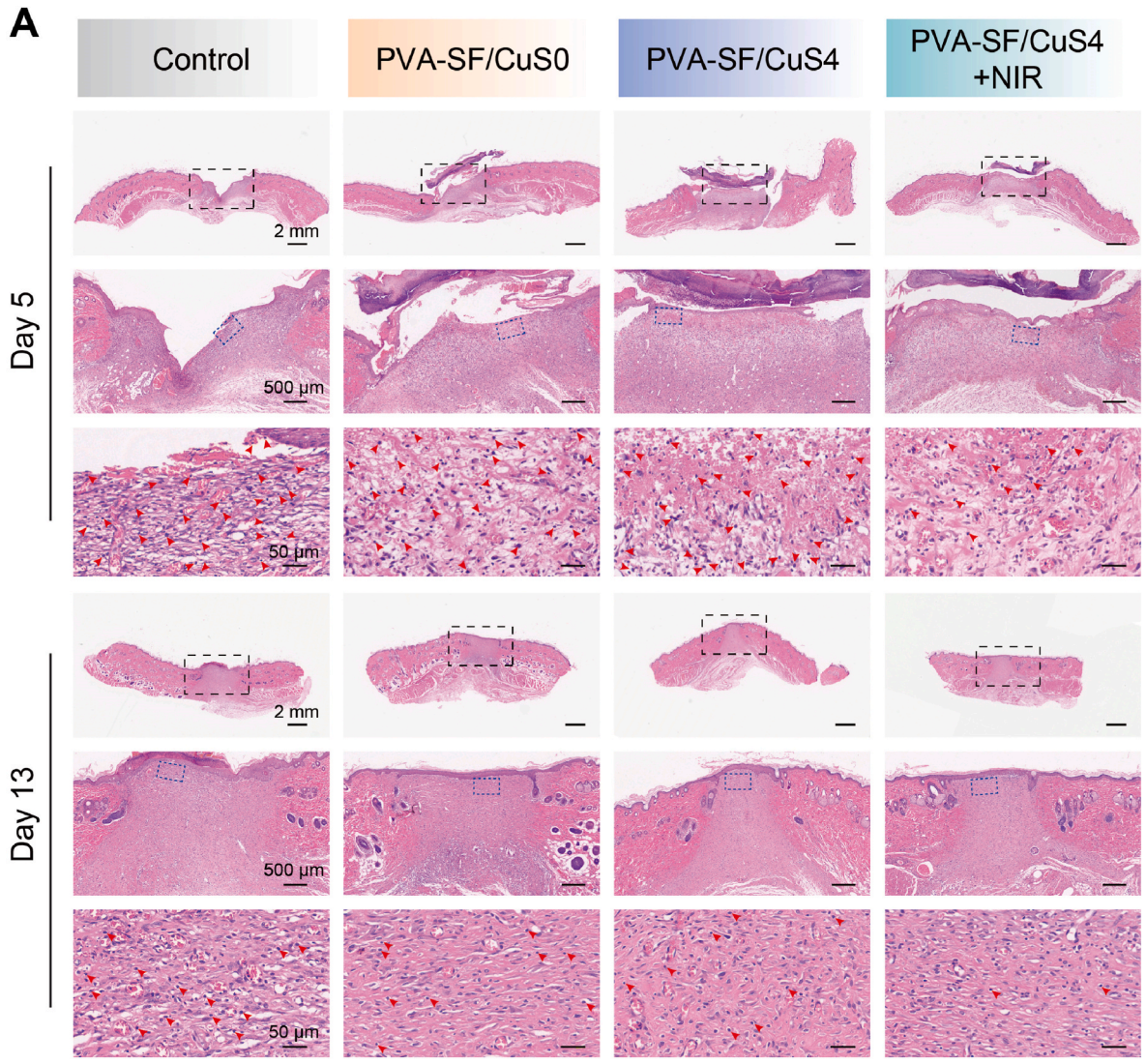

Fig. 10. H&E staining of PVA-SF/CuS nanofiber membrane in treating *S. aureus*-infected wounds.

Where ODS is the absorbance of the sample supernatant, ODP is the absorbance of the positive control, and ODN is the absorbance of the negative control.

2.12. In vivo wound healing

SD rats were obtained from the Animal Experiment Center of Southwestern Medical University. All experiments were licensed by the Animal Ethics Committee of Southwest Medical University (20230703-007). Rats were randomly divided into four groups, and circular wounds of the same size and moderate depth were created at the same position on the rats' backs. The groups were as follows: 1) Blank control group: no treatment was applied to the wounds; 2) PVA-SF/CuS0 group: wounds were treated with PVA-SF/CuS0; 3) PVA-SF/CuS4 group: wounds were treated with PVA-SF/CuS4; 4) PVA-SF/CuS4+NIR group: wounds were treated with PVA-SF/CuS4, and daily NIR (808 nm near-infrared radiation) exposure was applied to the wounds for 2 min, with thermal imaging performed every 30 s to record temperature changes.

On days 0, 3, 5, 7, 9, 11, and 13, a camera was used to take images of the wound, and ImageJ was used to measure and record the wound area. On days 5 and 13, tissue sections were obtained from the wound sites and stained with H&E, Masson, CD31, and IL-6. Quantitative analysis was performed using ImageJ software for the stained tissues.

2.13. Statistical analysis

All data were processed and statistically analyzed by Origin software for data processing. Each experiment was implemented with at least 3 replications. Data were analyzed using a *t*-test and one-way ANOVA. Differences were considered statistically significant at $*p < 0.05$, $**p < 0.01$, and $***p < 0.001$.

3. Result and discussion

3.1. Characterization of SF/CuS NPs

It has been demonstrated that biomolecules containing many hydroxyl groups can synthesize CuS through the limiting threshold effect of the gap between hydroxyl groups [20]. Therefore, it is feasible to use hydroxyl-rich silk fibroin proteins as templates for synthesizing CuS NPs. As shown in Fig. 2A, the silk fibroin protein solution was colorless and transparent, and the $CuSO_4$ solution was blue; the solution was violet after the addition of $[Cu(NH_3)_4]^{2+}$ to silk fibroin proteins due to the interaction between Cu(II) ions and the silk fibroin molecular chain. After adding Na_2S, the solution was brown without precipitation, which

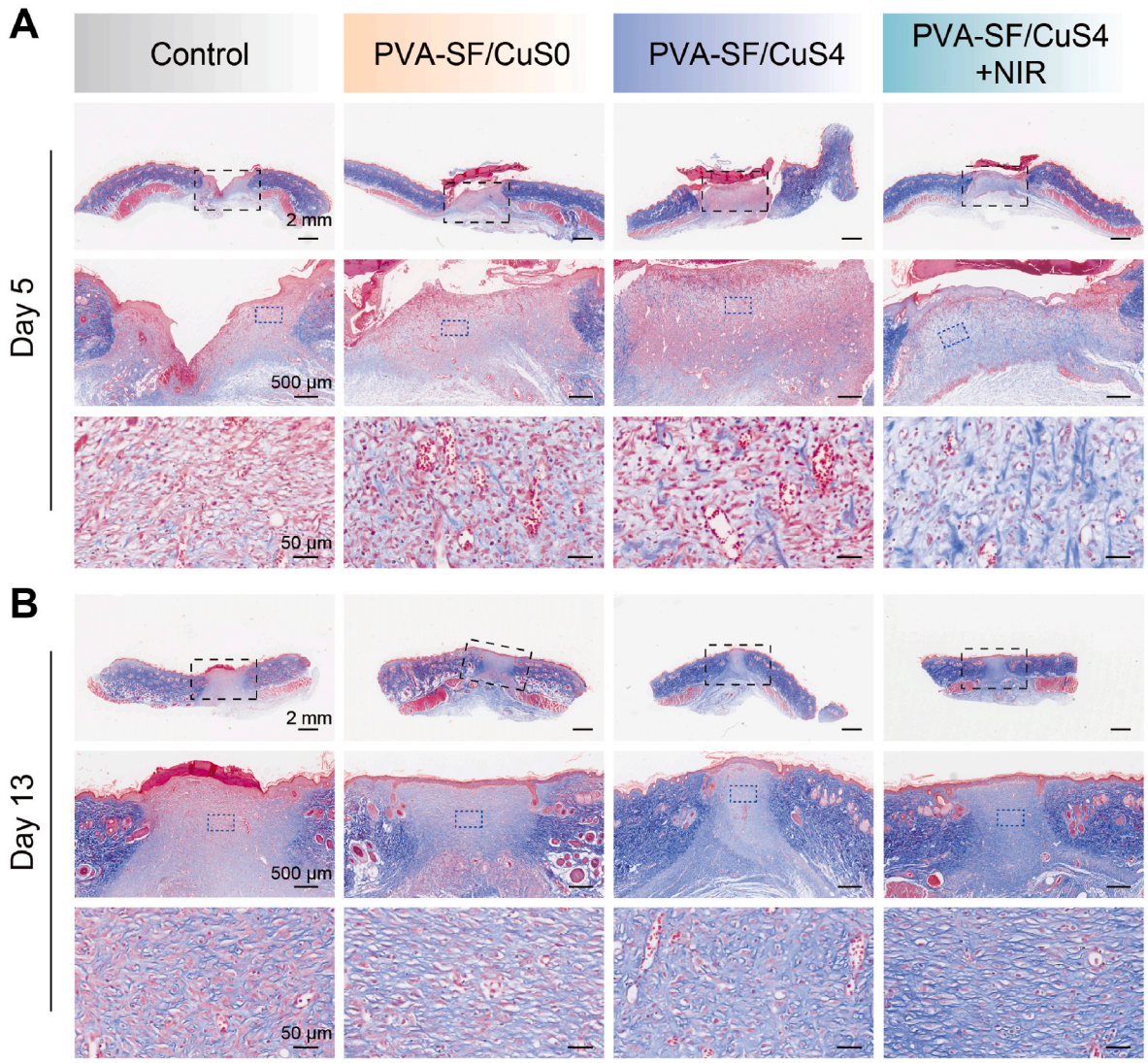

Fig. 11. Masson trichrome staining of PVA-SF/CuS nanofiber membrane in treating *S. aureus*-infected wounds.

was attributed to the complexation of Cu^{2+} with wealthy hydroxyl groups in the silk fibroin molecules.

The UV–Vis absorption spectroscopy shows that an absorption peak at 275 nm is observed in the silk fibroin protein solution (Fig. 2B), which is attributed to the π→π* jump of tyrosine residues in the SF macromolecule [46]. The SF/CuS NP solution showed significant absorption in the near-infrared region (700–1100 nm) (Fig. 2C), which is typical of CuS NP absorption, indicating its successful synthesis [47]. The absorption of SF/CuS NP solution in the NIR region was enhanced with increased Cu^{2+} concentration (Fig. 2D), consistent with the previous study [20].

The TEM results are shown in Fig. 2F, where the circular nanoparticles are well dispersed, and the nanoparticles have ordered lattice stripes with a lattice spacing of 0.34 nm, corresponding to the (101) crystal plane [48]. Statistical analysis of the particle size revealed that the particle size is about 10–20 nm (Fig. 2E), and these results indicate that SF/CuS NPs have good dispersion and colloidal stability in the solution. In addition, SF/CuS NPs exhibit distinct diffraction peaks corresponding to the standard hexagonal CuS phase card (JCPDS file No. 06–0464) (Fig. S1) [20]. Further EDS and XPS spectroscopy showed that the samples contained C, N, O, S, and Cu (Fig. 2G and H). The XPS spectra showed two independent peaks at 952.2 eV and 931.6 eV (Fig. 2I), which were correlated with Cu $2p_{1/2}$ and Cu $2p_{3/2}$ in Cu ions, respectively [49,50], which further demonstrated the successful synthesis of SF/CuS NPs. The TGA of SF and SF/CuS NPs is shown in Fig. S2. The first weight loss occurs at a temperature of 100 °C, which may be related to the evaporation of moisture in the sample. A significant weight loss is observed between 300 and 800 °C, which may be associated with the degradation of silk fibroin [20]. This demonstrates the excellent thermal stability of SF/CuS NPs.

3.2. Photothermal performance of SF/CuS NPs

SF/CuS NPs were irradiated with an 808 nm (1.8 W/cm^2) laser, and the temperature changes were monitored using a thermal imager to evaluate the photothermal conversion efficiency. As shown in Fig. 3A and B, it can be seen that under the same power condition (1.8 W/cm^2), the temperature of SF/CuS0 did not change significantly under laser irradiation, which indicated that SF did not have a photothermal effect. However, the temperature of SF/CuS0.5, SF/CuS1, SF/CuS2, and SF/CuS4 increased by 19.4 °C, 43.5 °C, and 59.2 °C, respectively, which indicated that the photothermal conversion performance was available for SF/CuS NPs and the photothermal conversion efficiency increases with the concentration of SF/CuS. At the same SF/CuS NP concentration, the higher the light power, the higher the photothermal conversion efficiency (Fig. 3C). Further, switching cycle experiments were performed to analyze the photothermal stability of SF/CuS NPs, as shown in Fig. 3D, after three switching cycles, the SF/CuS NP solution can still rise

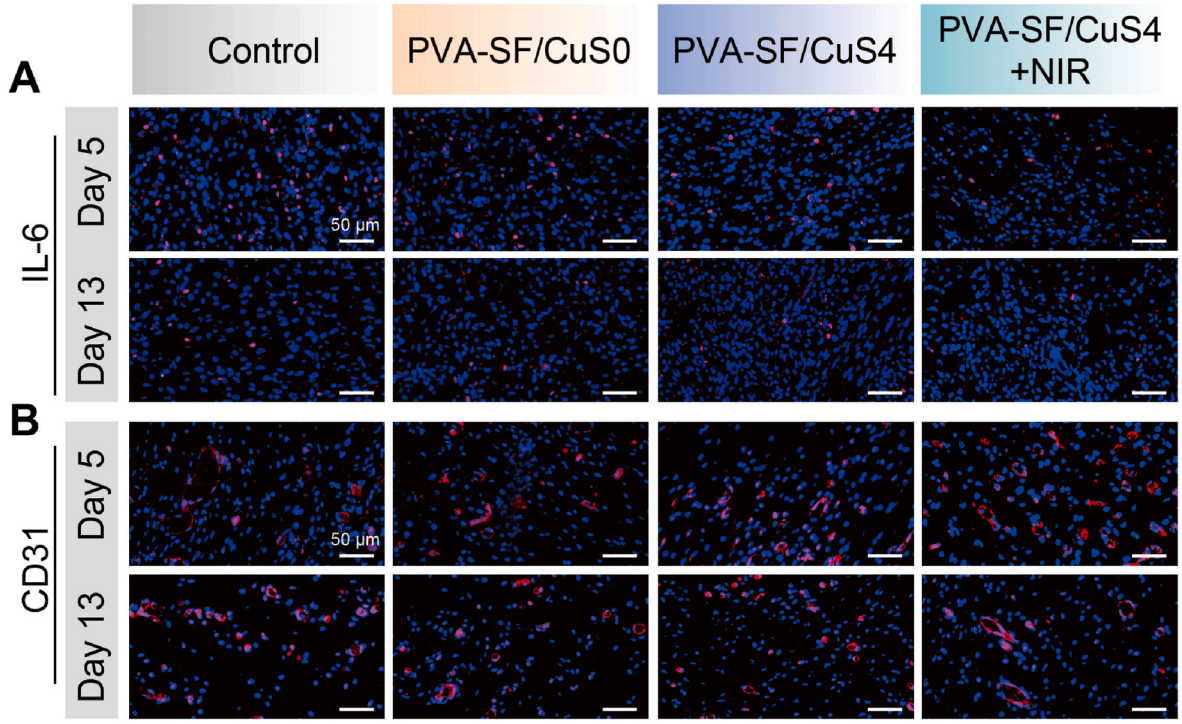

Fig. 12. (A) IL-6 and (B) CD31 immunofluorescence staining of PVA-SF/CuS nanofiber membrane in treating *S. aureus*-infected wounds.

to the previous temperature, indicating its good photothermal stability. These results suggest that SF/CuS NPs have excellent photothermal performance and photothermal stability.

3.3. Morphology and properties of PVA-SF/CuS composite membranes

Electrostatically spun nanofibers have received increasing attention in medical applications as they can provide an ideal biomimetic environment for wound healing [36,51]. Polyvinyl alcohol (PVA) has been widely studied in tissue engineering due to its excellent biocompatibility, mechanical strength, and biodegradability, but it lacks bioactivity [52]. Silk fibroin is a natural protein that is hydrophilic and biocompatible [53]. Therefore, we chose PVA and SF as the substrates for nanofiber membranes loaded with SF/CuS NPs. SEM images showed that all the membranes consisted of randomly stacked, smooth nanofibers (Fig. 4A), and the incorporation of SF/CuS NPs did not affect the morphology of the nanofiber membranes. Energy dispersive x-ray spectroscopy (EDS) mapping analysis showed that elemental sulfur and copper were uniformly distributed in the nanofiber membranes (Fig. 4B), indicating the successful loading and uniform dispersion of SF/CuS NPs in the nanofiber membranes.

FTIR spectra showed characteristic peaks of PVA at 3257, 1415, and 1081 cm^{-1}, which are attributed to O-H, C-H, and C-O stretching vibrations, respectively [29]. The silk fibroin showed strong bands at 1635, 1516, and 1236 cm^{-1}, corresponding to the characteristic peaks of amide I, II, and III [44]. The distinctive peaks of PVA and silk fibroin protein were observed for PVA-SF/CuS, indicating the presence of silk fibroin and PVA (Fig. 4C). The FTIR spectrum of CuS shows a peak at 623 cm^{-1}, which is due to the stretching vibration of Cu-S [19,54]. The characteristic peaks of PVA, silk fibroin, and Cu-S were observed in PVA-SF/CuS4, indicating the successful loading of SF/CuS NPs. Further, nanofibrous membranes loaded with different concentrations of CuS were subjected to contact angle experiments (Fig. 4D), and all the fibrous membranes were hydrophilic with no significant difference in the contact angle, suggesting that SF/CuS addition does not affect the hydrophilicity of the nanofibrous membranes.

The biodegradability of nanofiber membranes is essential if they are to be used as biomaterials [55]. In clinical practice, nanofiber membranes used for wound dressings are usually replaced every two days. We, therefore, immersed the nanofiber films in PBS for five days and observed the changes in their appearance and quality, respectively (Fig. S3). The results showed that the relative mass of each group of nanofibers was still more than 90 % after 5 Days of immersion, indicating that the nanofiber film has good stability, which is beneficial for application in wound repair.

3.4. Photothermal performance of PVA-SF/CuS nanofiber membranes

To verify the photothermal performance of PVA-SF/CuS nanofiber membranes, they were irradiated by an 808 nm (1.0 w/cm^2) laser for 2 min, and the temperature change was monitored using a thermography camera to evaluate the photothermal conversion efficiency. As shown in Fig. 5A and B, under the same power condition (1.0 w/cm^2), after experiencing 2 min of laser irradiation, there was no significant change in the temperature of the PVA-SF/CuS0 group. However, the temperatures of PVA-SF/CuS0.5, PVA-SF/CuS1, PVA-SF/CuS2, and PVA-SF/CuS4 increased with the increase in the concentration of CuS in the nanofiber membranes, which reached 34.4, 45.4, 50.3, and 54.5 °C, respectively, indicating that the incorporation of CuS NPs endowed the nanofiber membrane with excellent photothermal performance. The photothermal conversion efficiency of PVA-SF/CuS4 increased with higher light power (Fig. 5C). After 2 min of irradiation at 1.0 w/cm^2, the temperature of PVA-SF/CuS4 was 54.5 °C, which satisfied the antimicrobial demand without causing damage to the wound [56]. The stability of the photothermal conversion performance of PVA-SF/CuS4 was further examined. The results are shown in Fig. 5D; after five switching cycles, PVA-SF/CuS4 can still rise to the previous temperature, indicating good photothermal stability.

3.5. Antibacterial performances

Thermal therapy at temperatures above 50 °C can cause thermal damage to bacterial enzymes and proteins, which can inhibit or kill the bacteria [57,58]. *In vitro* photothermal antibacterial activity of

nanofiber was examined using *E. coli* as a Gram-negative and *S. aureus* as a Gram-positive model bacteria [59]. The groups not exposed to NIR light had no antimicrobial properties (Fig. 6A–C). When irradiated by 808 nm laser for 2 min, PVA-SF/CuS0 had no antimicrobial properties, PVA-SF/CuS0.5, PVA-SF/CuS1 and PVA-SF/CuS2 had slight antimicrobial properties, PVA-SF/CuS4 had the best antimicrobial properties compared with the control group, and the *S. aureus* and *E. coli* with survival rates of 0.6 % and 1 %, respectively (Fig. 6B–D).

Antibacterial performance was further assessed using the Live/Dead Bacterial Viability Kit [60]. As shown in Fig. 6E and F, the groups without NIR and the PVA-SF/CuS0+NIR group of bacteria showed green fluorescence, indicating bacterial survival and no antimicrobial performance. In the presence of NIR, red fluorescence was observed in PVA-SF/CuS0.5, PVA-SF/CuS1, and PVA-SF/CuS2 groups, indicating that some bacteria were killed. Meanwhile, the PVA-SF/CuS4+NIR group showed almost complete red fluorescence, indicating that the bacteria were virtually destroyed. These results suggest that the excellent NIR antibacterial activity of the nanofiber membrane is related to the content of CuS and that after 808 nm laser irradiation, the PVA-SF/CuS4 nanofiber membrane possesses excellent antimicrobial capacity.

3.6. Cell cytocompatibility

The biocompatibility of nanofiber membranes is crucial for their biomedical applications [61]. Here, we first examined the cytocompatibility of nanofiber membranes by co-culturing PVA-SF/CuS nanofiber membrane extracts with L929 and HUVECs cells for 1, 3, and 5 days, respectively, and then performing live/dead cell staining and CCK-8 analysis. The live/dead cell staining results were shown in Fig. 7A and B, cells in both PVA-SF/CuS0 and PVA-SF/CuS4 groups showed green fluorescence and were not different from the control group. The CCK-8 results showed that the cell viability of the PVA-SF/CuS0 and PVA-SF/CuS4 groups exhibited an increasing trend on days 1, 3, and 5. There was no significant difference compared to the control group (Fig. 7C and D), which indicated that the PVA-SF/CuS4 fiber membrane has excellent biocompatibility and no cytotoxicity.

In addition, the cells were co-cultured with the fibrous membrane extract for 3 days, and then cell morphology was observed. FITC-Phalloidin staining showed the L929 cells morphological no significant difference between the control, PVA-SF/CuS0, and PVA-SF/CuS4 groups (Fig. 8A). Similarly, the morphology of HUVEC cells treated in the PVA-SF/CuS0 and PVA-SF/CuS4 groups was not significantly different from the control group (Fig. 8B). These results further indicated that the PVA-SF/CuS nanofiber membrane had good biocompatibility.

The PVA-SF/CuS fiber membrane extracts were further co-cultured with erythrocytes for 1 h to test their hemocompatibility. The erythrocytes in the positive control group (TritonX-100) were all ruptured and showed apparent hemolysis. However, erythrocyte morphology in the PVA-SF/CuS0 and PVA-SF/CuS4 groups was unchanged (Fig. 8C and D). The hemolysis rate results for the PVA-SF/CuS0 and PVA-SF/CuS4 groups showed less than 5 % (Fig. 8E), which is the threshold for the international standard hemolysis rate [62]. In all, these results indicated that the PVA-SF/CuS4 nanofiber membrane had excellent hemocompatibility.

3.7. Wound healing and histological analysis of infected wounds in rats

We established whole skin defects on SD rat skin to evaluate the effect of PVA-SF/CuS nanofibrous membranes in promoting infected wound healing *in vivo*. As shown in Fig. 9A, after establishing the rat skin wound model, *S. aureus* was dropped into the wounds, and the infected wounds were treated with PBS, PVA-SF/CuS0, PVA-SF/CuS4, and PVA-SF/CuS4+NIR, respectively. After irradiating the wound with an 808 nm NIR laser (1 W/cm^2) for 2 min, the temperature of the PVA-SF/CuS4 nanofiber membrane increased to 51.5 °C (Fig. 9B), a temperature that kills bacteria without damaging the tissue [56]. Fig. 9C shows the images of the changes in the wounds on days 0, 3, 7, and 13, and found that the PVA-SF/CuS4+NIR group showed faster wound healing throughout the treatment process than all other groups; the PVA-SF/CuS0 and PVA-SF/CuS4 groups showed faster wound healing than the control group. Quantitative and statistical analyses of the wound area at each time point were performed (Fig. 9D and E), and the ratio of the remaining wound area in the PVA-SF/CuS4+NIR group was significantly smaller than that in the other groups. The corresponding ratio of wound healing area in the PVA-SF/CuS4+NIR group was considerably higher than in other groups, mainly due to the photothermal responsive properties of PVA-SF/CuS4 under near-infrared laser irradiation, which kills bacteria in the wound, thereby reducing the inflammatory response and accelerating wound healing.

There are diverse reports in the literature on composite CuS NPs and the synthetic methodologies of the aim antimicrobial potential and biomedical properties, which mainly have used diverse strategies (Table S1) [63–66]. In contrast to these approaches in the literature, in our work, the synthesis of copper sulfide by using silk fibroin as a template and ensuring uniform dispersion and stability of copper sulfide nanoparticles provides a green and facile approach. Unlike synthesis methods that rely heavily on chemical reagents that may be harmful to health, our method is green and does not generate toxic byproducts. In addition, a nanofiber dressing with excellent photo-thermal responsive antimicrobial properties and excellent biocompatibility was prepared by uniquely combining silk fibroin and CuS NPs with PVA *via* electrospinning. The results of the *in vivo* study showed accelerated wound healing, exceeding the results reported in other studies.

3.8. Histopathological analysis

H&E and Masson staining further assessed the wound-healing effect of the nanofiber membrane. The H&E results are shown in Fig. 10. On the 5th day, the control group and PVA-SF/CuS0 group showed no new epidermal layer and significant inflammatory cells; the PVA-SF/CuS4 group showed a newly formed epidermal layer, but still had a large number of inflammatory cells; the PVA-SF/CuS4+NIR group showed a newly formed epidermal layer with a small amount of inflammatory cells and the formation of blood vessels. On the 13th day, the control group showed visible neo-epidermis and crusting, and inflammatory cells were still present. However, the epidermal layer in the PVA-SF/CuS4+NIR group was similar in thickness to the intact epidermal layer, and the tissues were arranged regularly. These results indicate that PVA-SF/CuS4 under NIR light can effectively shorten the duration of inflammatory response and promote wound repair.

Collagen is an essential component of fibrous connective tissue, and its deposition and reconstitution in the area of the defect is another critical indicator of wound healing [67]. Masson trichrome staining was used to detect collagen formation in the wound tissue, and the blue color represents the newborn collagen fibers. As shown in Fig. 11, more collagen deposition and neater collagen alignment were observed in the PVA-SF/CuS4+NIR group compared with all other groups, indicating that the PVA-SF/CuS4+NIR group accelerated the formation of collagen fibers, thus effectively promoting wound healing.

3.9. Immunofluorescence analysis

During wound healing, cytokine-regulated cellular activity affects the wound healing process. Interleukin-6 (IL-6) is a pro-inflammatory cytokine closely associated with the inflammatory response [68], and CD31 is a standard vascular endothelial cell marker used to characterize angiogenesis in wounds [69]. Therefore, we selected IL-6 and CD31 as indicators to evaluate the effectiveness of the nanofibrous membrane in wound healing. Immunofluorescence staining showed that the expression level of IL-6 in the PVA-SF/CuS4+NIR group was significantly lower than that in the other three groups (Fig. 12A), suggesting that

PVA-SF/CuS4 was effective in reducing the inflammatory response under NIR. The immunofluorescence results of CD31 are shown in Fig. 12B; compared with the other groups, the highest expression of CD31 was observed on the 5th day in the PVA-SF/CuS4+NIR group, indicating that the PVA-SF/CuS4+NIR induced more vascularization. These results suggest that PVA-SF/CuS4+NIR accelerates the healing of infected wounds by reducing inflammation and promoting angiogenesis.

4. Conclusions

In summary, we have prepared silk fibroin-copper sulfide nanoparticles (SF/CuS NPs) with excellent dispersibility and photothermal properties by a simple and environmentally friendly method using silk fibroin as a biological template. Subsequently, these SF/CuS NPs were mixed with PVA and silk fibroin solutions to prepare PVA-SF/CuS nanofibrous membranes by electrostatic spinning. PVA-SF/CuS nanofibrous membranes have good biocompatibility and low cytotoxicity, and they have an excellent photothermal bacterial killing effect under near-infrared laser irradiation. *In vivo* experiments confirmed that PVA-SF/CuS nanofiber membrane could promote the healing of infected full-thickness skin wounds in rats under near-infrared light irradiation. The histological results showed that the PVA-SF/CuS nanofiber membrane could effectively inhibit the expression of pro-inflammatory factor (IL-6), promote the expression of the angiogenic factor (VEGF), and accelerate collagen deposition and neovascularization, thus accelerating the healing of infected wounds. Therefore, our prepared photothermal nanofiber membrane provides a new material for the future treatment of infected wounds and bacterial diseases. Moreover, the versatility and potential of this approach could be expanded to other areas, such as tissue engineering and chronic wound management, where infection control and accelerated healing are critical. Future studies may explore its clinical application, including tailored therapies for infections and personalized treatments for individual patients.

CRediT authorship contribution statement

Rui Cai: Writing – original draft, Visualization, Investigation, Formal analysis, Data curation. **Jiayu Zhao:** Writing – original draft, Visualization, Investigation, Data curation. **Peirong Zhou:** Methodology, Formal analysis. **Xuemin Ma:** Methodology, Formal analysis. **Chuankai Zhang:** Methodology, Formal analysis. **Zhaodan Wu:** Visualization, Investigation, Formal analysis. **Liyu Hu:** Visualization, Investigation, Formal analysis. **Yajuan Hu:** Visualization, Investigation, Formal analysis. **Yongcen Chen:** Visualization, Investigation, Formal analysis. **Chenglong Huang:** Writing – review & editing, Visualization, Formal analysis. **Gang Tao:** Writing – review & editing, Visualization, Methodology, Investigation, Funding acquisition, Data curation.

Declaration of competing interest

The authors declare no conflict of interest. The founding sponsors had no role in the design of the study and in the decision to publish the results.

Acknowledgements

This work was funded by Sichuan Science and Technology Program (2024NSFSC1655), Health Commission of Sichuan Province Medical Science and Technology Program (24QNMP094), Luzhou Science and Technology Program (2023JYJ030, 2023SYF101), The Special Research Project for Wound Disease (Taige) and Sichuan Medical Association (2023TG08), Sichuan Province Medical Youth Innovation Research Project (Q23010), Xuzhou District People's Government-Southwest Medical University Cooperation Project (2021XZXNYD03), Scientific Research Foundation of Southwest Medical University (2023ZD002), Project of Stomatological Institute of Southwest Medical University (2021XJYJS01), Scientific Research Foundation of the Affiliated Stomatological Hospital of Southwest Medical University (2024KQZX12, 2023BS01, 2023KQ03, 2023Z01).

Appendix A. Supplementary data

Supplementary data to this article can be found online at https://doi.org/10.1016/j.mtbio.2025.101605.

Data availability

Data will be made available on request.

References

[1] S. Zhang, H. Yang, M. Wang, D. Mantovani, K. Yang, F. Witte, L. Tan, B. Yue, X. Qu, Immunomodulatory biomaterials against bacterial infections: progress, challenges, and future perspectives, Innovation (2023) 100503.
[2] X. Tang, X. Wang, Y. Sun, L. Zhao, D. Li, J. Zhang, H. Sun, B. Yang, Magnesium oxide-assisted dual-cross-linking bio-multifunctional hydrogels for wound repair during full-thickness skin injuries, Adv. Funct. Mater. 31 (43) (2021) 2105718.
[3] Y. Yang, M. Li, G. Pan, J. Chen, B.L. Guo, Multiple stimuli-responsive nanozyme-based cryogels with controlled NO release as self-adaptive wound dressing for infected wound healing, Adv. Funct. Mater. 33 (31) (2023) 2214089.
[4] Y. Yang, Y. Liang, J. Chen, X. Duan, B. Guo, Mussel-inspired adhesive antioxidant antibacterial hemostatic composite hydrogel wound dressing via photo-polymerization for infected skin wound healing, Bioact. Mater. 8 (2022) 341–354.
[5] Y.J. Fu, R.K. Wang, C.Y. Ma, L.Y. Wang, S.Y. Long, K. Li, X. Zhao, W. Yang, Injectable oxygen-carrying microsphere hydrogel for dynamic regulation of redox microenvironment of wounds, Small (2024) 2403781.
[6] J. Jiang, X. Lv, H. Cheng, D. Yang, W. Xu, Y. Hu, Y. Song, G. Zeng, Type I photodynamic antimicrobial therapy: principles, progress, and future perspectives, Acta Biomater. 177 (2024) 1–19.
[7] R.A. Salman, S.K. Jameel, S.M. Shakir, Study of antimicrobial activity of silver nanoparticles against *Salmonella typhi* infections *in vitro*, Journal of Medicinal and Chemical Sciences 6 (2023) 733–745.
[8] A.J. Uttu, M.S. Sallau, O.R.A. Iyun, H. Ibrahim, Recent advances in isolation and antimicrobial efficacy of selected strychnos species: a mini review, Journal of Chemical Reviews 4 (2022) 59–62.
[9] J. Li, X. Xu, X. Ma, M. Cui, X. Wang, J. Chen, J. Zhu, J. Chen, Antimicrobial nonisocyanate polyurethane foam derived from lignin for wound healing, ACS Appl. Bio Mater. 7 (2) (2024) 1301–1310.
[10] Y. Liu, L. Zhang, F. Ouyang, C. Xue, X. Zhao, T. Wang, Z. Pei, Q. Shuai, Thermal-accelerated urease-driven bowl-like polydopamine nanorobot for targeted photothermal/photodynamic antibiotic-free antibacterial therapy, Adv. Healthcare Mater. (2024) 2304086.
[11] M. Du, X. He, D. Wang, Z. Jiang, X. Zhao, J. Shen, An NIR-II-enhanced nanozyme to promote wound healing in methicillin-resistant Staphylococcus aureus infections, Acta Biomater. 179 (2024) 300–312.
[12] S.T. Dibaba, R. Caputo, W. Xi, J.Z. Zhang, R. Wei, Q. Zhang, J. Zhang, W. Ren, L. Sun, NIR light-degradable antimony nanoparticle-based drug-delivery nanosystem for synergistic chemo–photothermal therapy in vitro, ACS applied materials interfaces 11 (51) (2019) 48290–48299.
[13] L. Li, G. Zhu, W. Xu, M. Wang, Y. Xie, Z. Bao, M. Qi, M. Gao, C. Li, Construction of mPt/ICG-αA nanoparticles with enhanced phototherapeutic activities for multidrug-resistant bacterial eradication and wound healing, Nanoscale 15 (33) (2023) 13617–13627.
[14] C. Lee, Enhancing photothermal therapy via blood clot induced by needle-type sodium hydroxide-loaded starch implant, Colloid Interface Science Communications 59 (2024) 100773.
[15] X. Fu, Y. Song, X. Feng, Z. Liu, W. Gao, H. Song, Q. Zhang, Synergistic chemotherapy/PTT/oxygen enrichment by multifunctional liposomal polydopamine nanoparticles for rheumatoid arthritis treatment, Asian J. Pharm. Sci. (2024) 100885.
[16] X. Zhan, J. Yan, D. Xiang, H. Tang, L. Cao, Y. Zheng, H. Lin, D. Xia, Near-infrared light responsive gold nanoparticles coating endows polyetheretherketone with enhanced osseointegration and antibacterial properties, Materials Today Bio 25 (2024) 100982.
[17] Y. Guo, C. Zhang, B. Xie, W. Xu, Z. Rao, P. Zhou, X. Ma, J. Chen, R. Cai, G. Tao, Y. He, Multifunctional microneedle patch based on metal-phenolic network with photothermal antimicrobial, ROS scavenging, immunomodulatory, and angiogenesis for programmed treatment of diabetic wound healing, ACS Appl. Mater. Interfaces. 16 (26) (2024) 33205–33222.
[18] M.A. Turkia, T.A. Salman, A review on the synthesis of nanomaterials: comparing traditional and biological green methods, Journal of Chemical Reviews 6 (4) (2024) 458–481.
[19] Y. Guo, B. Xie, M. Jiang, L. Yuan, X. Jiang, S. Li, R. Cai, J. Chen, X. Jiang, Y. He, Facile and eco-friendly fabrication of biocompatible hydrogel containing CuS@ Ser NPs with mechanical flexibility and photothermal antibacterial activity to promote infected wound healing, J. Nanobiotechnol. 21 (1) (2023) 266.
[20] H. Chen, N. Yu, J. Wang, S. Zhang, L. Cao, M. Zhou, Z. Xu, S. Lin, S. Yin, X. Jiang, Construction of versatile fibroin/nanozyme hybrid microneedles with controllable

phototherapeutic sterilization property against periodontitis, Nano Today 56 (2024) 102297.
[21] Z. Li, X. Huang, L. Lin, Y. Jiao, C. Zhou, Z. Liu, Polyphenol and Cu2+ surface-modified chitin sponge synergizes with antibacterial, antioxidant and pro-vascularization activities for effective scarless regeneration of burned skin, Chem. Eng. J. 419 (2021) 129488.
[22] G.Y. Huang, W.J. Chang, T.W. Lu, I.L. Tsai, S.J. Wu, M.H. Ho, F.L. Mi, Electrospun CuS nanoparticles/chitosan nanofiber composites for visible and near-infrared light-driven catalytic degradation of antibiotic pollutants, Chem. Eng. J. 431 (2022) 134059.
[23] H. Zhao, Z.X. Liang, Z.Z. Gao, Facile preparation of floatable carboxymethyl cellulose-based composite hydrogel for efficient removal of organic dyes, Colloid Interface Science Communications 49 (2022) 100637.
[24] C. Bhuvaneswari, S.G. Babu, Nanoarchitecture and surface engineering strategy for the construction of 3D hierarchical CuS-rGO/g-C3N4 nanostructure: an ultrasensitive and highly selective electrochemical sensor for the detection of furazolidone drug, J. Electroanal. Chem. 907 (2022) 116080.
[25] Y. Chen, R. Su, F. Wang, W. Zhou, B. Gao, Q. Yue, Q. Li, In-situ synthesis of CuS@ carbon nanocomposites and application in enhanced photo-fenton degradation of 2, 4-DCP, Chemosphere 270 (2021) 129295.
[26] G. Tao, R. Cai, Y. Wang, L. Liu, H. Zuo, P. Zhao, A. Umar, C. Mao, Q. Xia, H. He, Bioinspired design of AgNPs embedded silk sericin-based sponges for efficiently combating bacteria and promoting wound healing, Mater. Des. 180 (2019) 107940.
[27] M. Jiang, S. Li, P. Ming, Y. Guo, L. Yuan, X. Jiang, Y. Liu, J. Chen, D. Xia, Y. He, Rational design of porous structure-based sodium alginate/chitosan sponges loaded with green synthesized hybrid antibacterial agents for infected wound healing, Int. J. Biol. Macromol. 237 (2023) 123944.
[28] P. Ming, Y. Liu, P. Yu, X. Jiang, L. Yuan, S. Cai, P. Rao, R. Cai, X. Lan, G. Tao, A biomimetic Se-nHA/PC composite microsphere with synergistic immunomodulatory and osteogenic ability to activate bone regeneration in periodontitis, Small 20 (9) (2024) 2305490.
[29] W. Li, Z. Wu, J. Zhao, M. Jiang, L. Yuan, Y. Guo, S. Li, L. Hu, X. Xie, Y. Zhang, Fabrication of dual physically cross-linked polyvinyl alcohol/agar hydrogels with mechanical stability and antibacterial activity for wound healing, Journal of Biological Macromolecules 247 (2023) 125652.
[30] C. Zhang, J. Chai, Q. Jia, J. Tan, Z. Meng, N. Li, M. Yuan, Evaluating the therapeutic efficacy of radiolabeled BSA@ CuS nanoparticle-induced radio-photothermal therapy against anaplastic thyroid cancer, IUBMB Life 74 (5) (2022) 433–445.
[31] J. Liu, X. Xie, T. Wang, H. Chen, Y. Fu, X. Cheng, J. Wu, G. Li, C. Liu, H. Liimatainen, Promotion of wound healing using nanoporous silk fibroin sponges, ACS Appl. Mater. Interfaces 15 (10) (2023) 12696–12707.
[32] H.A. Tran, T.T. Hoang, A. Maraldo, T.N. Do, D.L. Kaplan, K.S. Lim, J. Rnjak-Kovacina, Emerging silk fibroin materials and their applications: new functionality arising from innovations in silk crosslinking, Mater. Today 65 (2023) 244–259.
[33] M. Zhang, X. Zhao, Alginate hydrogel dressings for advanced wound management, Journal of Biological Macromolecules 162 (2020) 1414–1428.
[34] L. Yuan, X. Jiang, M. Jiang, Y. Guo, Y. Liu, P. Ming, S. Li, P. Zhou, R. Cai, K. Yu, G. Tao, Design, Biocompatible gellan gum/sericin hydrogels containing halloysite@ polydopamine nanotubes with hemostasis and photothermal antibacterial properties for promoting infectious wound repair, Mater. Des. 227 (2023) 111744.
[35] S. Li, M. Jiang, Y. Zhang, X. Xie, W. Li, P. Ming, X. Jiang, B. Yang, Y. He, J. Chen, G. Tao, Multi-functional carboxymethyl chitosan/sericin protein/halloysite composite sponge with efficient antibacterial and hemostatic properties for accelerating wound healing, Journal of Biological Macromolecules 234 (2023) 123357.
[36] Y. Yang, Y. Du, J. Zhang, H. Zhang, B. Guo, Structural and functional design of electrospun nanofibers for hemostasis and wound healing, Advanced Fiber Materials 4 (5) (2022) 1027–1057.
[37] H. Wu, J. Fan, C.-C. Chu, J.M. Wu, Electrospinning of small diameter 3-D nanofibrous tubular scaffolds with controllable nanofiber orientations for vascular grafts, ournal of Materials Science: Materials in Medicine 21 (2010) 3207–3215.
[38] X. Gao, S. Han, R. Zhang, G. Liu, J. Wu, Progress in electrospun composite nanofibers: composition, performance and applications for tissue engineering, J. Mater. Chem. B 7 (45) (2019) 7075–7089.
[39] J. Lee, E. Kim, K.J. Kim, J.W. Rhie, K.I. Joo, H.J. Cha, Protective topical dual-sided nanofibrous hemostatic dressing using mussel and silk proteins with multifunctionality of hemostasis and anti-bacterial infiltration, Small (2024) 2308833.
[40] Q. Chen, X. Wang, J. Liang, T. Zhang, X. Jiang, P. Liu, Technology, Synthesis of PVA@ S-BNNSs flexible fiber backbone by electrostatic spinning assisting the construction of excellent ductile epoxy thermal interface materials, Composites Science 247 (2024) 110435.
[41] H. Liu, R. Chen, P. Wang, J. Fu, Z. Tang, J. Xie, Y. Ning, J. Gao, Q. Zhong, X. Pan, Electrospun polyvinyl alcohol-chitosan dressing stimulates infected diabetic wound healing with combined reactive oxygen species scavenging and antibacterial abilities, Carbohydr. Polym. 316 (2023) 121050.
[42] H. Wang, Z. Xu, Q. Li, J. Wu, Application of metal-based biomaterials in wound repair, Engineered Regeneration 2 (2021) 137–153.
[43] H. Wang, Z. Xu, M. Zhao, G. Liu, J. Wu, Advances of hydrogel dressings in diabetic wounds, Biomater. Sci. 9 (5) (2021) 1530–1546.
[44] Y. Liu, C. Shi, P. Ming, L. Yuan, X. Jiang, M. Jiang, R. Cai, X. Lan, J. Xiao, G. Tao, Biomimetic fabrication of sr-silk fibroin co-assembly hydroxyapatite based microspheres with angiogenic and osteogenic properties for bone tissue engineering, Materials Today Bio (2024) 101011.
[45] X. Jiang, L. Yuan, P. Ming, M. Jiang, Y. Guo, S. Li, Y. Liu, C. Zhang, Z. Rao, J. Chen, Y. He, R. Cai, G. Tao, Muscle-inspired lamellar chitosan sponge with photothermal antibacterial and antioxidant properties for hemostasis and accelerated bacteria infected wound healing, Appl. Mater. Today 35 (2023) 101992.
[46] P. Nilogal, G.B. Uppine, R. Rayaraddi, H.K. Sanjeevappa, L.J. Martis, B. Narayana, S. Yallappa, Conductive in situ reduced graphene oxide–silk fibroin bionanocomposites, ACS Omega 6 (20) (2021) 12995–13007.
[47] Y. Nong, Y. Ren, P. Wang, M. Zhou, Y. Yu, J. Yuan, B. Xu, Q. Wang, A facile strategy for the preparation of photothermal silk fibroin aerogels with antibacterial and oil-water separation abilities, J. Colloid Interface Sci. 603 (2021) 518–529.
[48] R. Cai, H. Xiang, D. Yang, K.-T. Lin, Y. Wu, R. Zhou, Z. Gu, L. Yan, Y. Zhao, W. Tan, Plasmonic AuPt@ CuS heterostructure with enhanced synergistic efficacy for radiophotothermal therapy, J. Am. Chem. Soc. 143 (39) (2021) 16113–16127.
[49] H. Li, Y. Xiong, Y. Wang, W. Ma, J. Fang, X. Li, Q. Han, Y. Liu, C. He, P. Fang, High piezocatalytic capability in CuS/MoS2 nanocomposites using mechanical energy for degrading pollutants, J. Colloid Interface Sci. 609 (2022) 657–666.
[50] J. Hou, B. Huang, L. Kong, Y. Xie, Y. Liu, M. Chen, Q. Wang, One-pot hydrothermal synthesis of CdS–CuS decorated TiO2 NTs for improved photocatalytic dye degradation and hydrogen production, Ceram. Int. 47 (21) (2021) 30860–30868.
[51] L. Fu, Q. Feng, Y. Chen, J. Fu, X. Zhou, C. He, Nanofibers for the immunoregulation in biomedical applications, Advanced Fiber Materials 4 (6) (2022) 1334–1356.
[52] H. Liu, L.-Y. Lu, Y. Zhang, J. Zhao, C. Liu, L. Zhu, Q. Li, S. Chen, Covalently cross-linked ultrastrong SiO 2-loaded polyvinyl alcohol fibers via microfluidic spinning, Nanoscale 16 (25) (2024) 12007–12012.
[53] N. Johari, A. Khodaei, A. Samadikuchaksaraei, R.L. Reis, S.C. Kundu, L. Moroni, Ancient fibrous biomaterials from silkworm protein fibroin and spider silk blends: biomechanical patterns, Acta Biomater. 153 (2022) 38–67.
[54] H. Li, M. Jensen, N. Wang, Y. Chen, Y. Gao, X. Chen, X. Li, CuxS/PAN 3D nanofiber mats as ultra-lightweight and flexible electromagnetic interference shielding materials, Macromol. Mater. Eng. 304 (12) (2019) 1900482.
[55] R.O. Kareem, N. Bulut, O. Kaygili, Hydroxyapatite biomaterials: a comprehensive review of their properties, structures, medical applications, and fabrication methods, J. Chem. Rev 6 (1) (2024) 1–26.
[56] L. Ma, Y. Zhou, Z. Zhang, Y. Liu, D. Zhai, H. Zhuang, Q. Li, J. Yuye, C. Wu, Chang, Multifunctional bioactive Nd-Ca-Si glasses for fluorescence thermometry, photothermal therapy, and burn tissue repair, Sci. Adv. 6 (32) (2020) eabb1311.
[57] Y. Liang, X. Zhao, T. Hu, B. Chen, Z. Yin, P.X. Ma, B. Guo, Adhesive hemostatic conducting injectable composite hydrogels with sustained drug release and photothermal antibacterial activity to promote full-thickness skin regeneration during wound healing, Small 15 (12) (2019) 1900046.
[58] P. Jia, Y. Zou, J. Jiang, CuS hybrid hydrogel for near-infrared-enhanced infected wound healing: a gelatin-assisted synthesis and direct incorporation strategy, ACS Appl. Mater. Interfaces 15 (19) (2023) 22929–22943.
[59] M.N. Abdullah, M. El Arbi, Silver nano loaded solanum nigrum with potential biological activities, J Chemical Methodologies 8 (8) (2024) 585–602.
[60] L. Zhou, F. Chen, Z. Hou, Y. Chen, X. Luo, Injectable self-healing CuS nanoparticle complex hydrogels with antibacterial, anti-cancer, and wound healing properties, Chem. Eng. J. 409 (2021) 128224.
[61] V. Gavande, S. Nagappan, B. Seo, W.-K. Lee, A systematic review on green and natural polymeric nanofibers for biomedical applications, Int. J. Biol. Macromol. (2024) 130135.
[62] H. Guo, S. Tan, J. Gao, L. Wang, Sequential release of drugs form a dual-delivery system based on pH-responsive nanofibrous mats towards wound care, J. Mater. Chem. B 8 (8) (2020) 1759–1770.
[63] X. Liu, J. Pan, Y. Lv, X. Wang, X. Ma, X. Zhang, G. Cai, Z. Dong, Near-infrared responsive polycaprolactone coatings for magnesium implants: photodynamic antibacterial and controllable dissolution, J. Magnesium Alloys (2024) 2213–9567.
[64] Y. Zhao, Y. Wu, Q. Xu, Y. Liu, Z. Song, H. Han, H2O2 self-supplying and GSH-depleting nanosystem for amplified NIR mediated-chemodynamic therapy of MRSA biofilm-associated infections, J. Nanobiotechnol. 22 (1) (2024) 117.
[65] Y. Sun, W. Zhang, Z. Luo, C. Zhu, Y. Zhang, Z. Shu, C. Shen, X. Yao, Y. Wang, X. Wang, ZnO-CuS/F127 hydrogels with multienzyme properties for implant-related infection therapy by inhibiting bacterial arginine biosynthesis and promoting tissue repair, Adv. Funct. Mater. (2024) 2415778.
[66] Z. Li, Y. Huang, J. Luo, J. Chen, S. Huang, X. Zhao, B. Guo, Antibacterial and antioxidant supramolecular nanocomposite hydrogel dressings with angiogenesis and photo-thermal effect for multidrug-resistant bacterial infected wound healing, Chem. Eng. J. 499 (2024) 156381.
[67] J. Huang, S. Heng, W. Zhang, Y. Liu, T. Xia, C. Ji, L. Zhang, Dermal extracellular matrix molecules in skin development, homeostasis, wound regeneration and diseases, Semin. Cell Dev. Biol. 128 (2022) 137–144.
[68] B. Zhao, Y. Ren, K. Zhang, Y. Dong, K. Wang, N. Zhang, J. Li, M. Yuan, J. Wang, Q. Tu, Hydroxypropyl methylcellulose reinforced bilayer hydrogel dressings containing L-arginine-modified polyoxometalate nanoclusters to promote healing of chronic diabetic wounds, Carbohydr. Polym. (2024) 122396.
[69] C. Xian, Z. Zhang, X. You, Y. Fang, J. Wu, Nanosized fat emulsion injection modulating local microenvironment promotes angiogenesis in chronic wound healing, Adv. Funct. Mater. 32 (32) (2022) 2202410.